Soft Matter

REVIEW

View Article Online
View Journal | View Issue

Check for updates

Cite this: *Soft Matter*, 2023, **19**, 588

Fluid manipulation *via* multifunctional lubricant infused slippery surfaces: principle, design and applications

Xinsheng Wang,[a] Haoyu Bai,[ab] Zhe Li[b] and Moyuan Cao *[ac]

Water-repellent interfaces with high performance have emerged as an indispensable platform for developing advanced materials and devices. Inspired by the pitcher plant, slippery liquid-infused porous surfaces (SLIPSs) with reliable hydrophobicity have proven to possess great potential for various applications in droplet and bubble manipulation, droplet energy harvesting, condensation, fog collection, anti-icing, and anti-biofouling due to their excellent properties such as persistent surface hydrophobicity, molecular smoothness, and fluidity. This review aims to introduce the development history of interaction between SLIPSs and fluids as well as the design principles, preparation methods, and various applications of some of the more typical SLIPSs. The fluid manipulation strategies of the slippery surfaces have been proposed including the wettability pattern, oriented micro-structure, and geometric gradient. At last, the application prospects of SLIPSs in various fields and the challenges in the design and fabrication of slippery surfaces are analyzed. We envision that this review can provide an overview of the fluid manipulating processes on slippery surfaces for researchers in both academic and industrial fields.

Received 26th November 2022,
Accepted 4th January 2023

DOI: 10.1039/d2sm01547a

rsc.li/soft-matter-journal

Published on 04 2023. Downloaded on 31.01.2026 01:32:34.

1 Introduction

Nature is an inexhaustible source of inspiration. By mimicking various biological surfaces in nature, various advanced functional materials and surfaces have been developed. For example, superhydrophobic surfaces capable of repelling liquids are mimicked from natural surfaces such as lotus leaves,[1–3] water strider's legs,[4,5] rose petals,[6,7] butterfly wings,[8] *etc.* in nature. However, superhydrophobic surfaces have several

[a] *School of Materials Science and Engineering, Smart Sensing Interdisciplinary Science Center, Nankai University, Tianjin, 300350, P. R. China. E-mail: mycao@nankai.edu.cn*
[b] *School of Chemical Engineering and Technology, Tianjin University, Tianjin, 300072, P. R. China*
[c] *Haihe Laboratory of Sustainable Chemical Transformations, Tianjin, 300072, P. R. China. E-mail: moyuan.cao@tju.edu.cn*

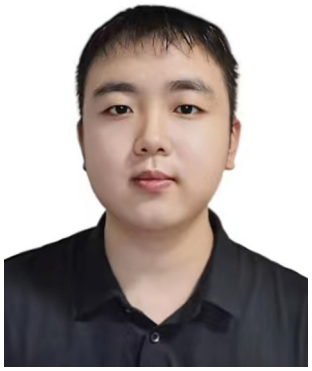

Xinsheng Wang

Xinsheng Wang is currently a PhD candidate at the School of Materials Science and Engineering, Nankai University, China. In 2019, he received his bachelor's degree in Chemical Engineering and Technology from North University of China. In 2022, he received his MS degree in Chemical Technology from Tianjin University. He joined Prof. Cao's lab in 2019 and his current research interests include lubricant-infused surfaces and fluid manipulation.

Haoyu Bai

Haoyu Bai is currently a PhD student at the School of Chemical Engineering and Technology, Tianjin University, China. In 2019, he received his bachelor's degree in Molecular Science and Engineering, which was jointly developed by Tianjin University and Nankai University. He joined Prof. Cao's lab in 2017, and his current research interests include fluid manipulation and steam collection with bio-inspired interfaces.

This journal is © The Royal Society of Chemistry 2023

Published on 04 2023. Downloaded on 31.01.2026 01:32:34.

disadvantages such as low mechanical stability, weak pressure stability, and short-term underwater stability, because the gas inside the micro-nano structure is easily contaminated and destroyed. A lubricant infused surface is an advanced functional surface inspired by the pitcher plant developed in recent years. Because of its excellent properties, such as liquid repellency, stability, smoothness, transparency, pressure resistance, *etc.* it has received a lot of attention. The pitcher plant is a special plant belonging to the tropics which has a unique organ for the uptake of nutrients. It consists of several structures with complex and ingenious surfaces (Fig. 2a).[9] The inner pitcher surface is divided into a lower glandular zone and an upper slippery zone. As shown in Fig. 2c, the slippery zone surface is porous and contains a layer of wax. And on the surface of the lower part of the plant, there are many glandular (Fig. 2d) as well as digestive juices.[1] The peristome surface of the pitcher is a compound anisotropic structure with a regular pattern, as shown in Fig. 2b, which enables directional droplet transport.[10] The peristome is surrounded by glands capable of emitting an aroma. When attracted insects explore the pitcher, the insects easily fall from the smooth slippery zone into the lower glandular zone containing the digestive fluid and perish. The reason this zone is so smooth is the presence of a stable layer of waxy liquid on its porous surface.

Inspired by this phenomenon, Professor Aizenberg's group reported the first demonstration of a bio-inspired slippery liquid infused porous surface (SLIPS) in 2011.[11] Based on the principle of surface energy matching, they infuse low-surface-tension perfluorinated liquids (3 M Fluorinert FC-70 or DuPont Krytox oils) into porous solid substrates to form a stable SLIPS surface. And this SLIPS has excellent liquid repellency that the hexane droplet could slide on its surface even with an inclination angle of only 3° (Fig. 2i). The SLIPS is composed of a liquid lubricant and a solid substrate (Fig. 2g). The substrate is generally porous or rough for the stability of the super-lubricated surface (Fig. 2h).[11,29–32] This structure combines the mechanical stability of a solid substrate with the molecularly smooth properties of a liquid surface, which gives the SLIPSs excellent characteristics such as self-healing, pressure resistance and long-lasting ability to repel liquids.[33] A brief history of the development of interaction between SLIPSs and fluids is shown in Fig. 1. We have listed some of the representative works and exhibited the evolution of the slippery surface. In this report, we present recent progress in the manufacture and application of multifunctional SLIPSs and reveal their design principles and physical-chemical essence. Finally, the future outlook and problems of SLIPSs are discussed. It should be noted that this review is aimed to introduce fluid-manipulation on SLIPS. Therefore, the detailed applications of slippery surfaces such as corrosion protection and biomedical usage are not fully covered. Some previous review articles were focused on such topics, and readers can find them in the ref. 33–37.

2 Design and fabrication of SLIPSs

2.1 Design principle

Superhydrophobic (SHB) surfaces inspired by lotus leaves are very common as a typical water-repellent surface in various production and experimental processes. Although SHB surfaces and SLIPSs are both water repelling surfaces, they are quite different. SHB surfaces repel water by an air film on their surface; however, SLIPSs repel water by means of a lubricant, *i.e.* by using one liquid to repel another (Fig. 3a); this also leads to the fact that the Cassie–Wenzel state transition to failure on superhydrophobic surfaces is not generally present on SLIPSs.[38] The behavior of the SLIPS is controlled by the interfacial interactions between the three phases (solid, lubricant, and repulsive fluid interactions and the surrounding environment) and the geometry of the solid surface.[39]

Zhe Li

Zhe Li is currently a PhD student at the School of Chemical Engineering and Technology, Tianjin University, China. In 2020, he received his MS degree in chemical technology from Tianjin University. He joined Prof. Cao's lab in 2017 and his current research interests are superhydrophobic surface preparation and its applications.

Moyuan Cao

Dr Moyuan Cao is currently a principal investigator at the School of Materials Science and Engineering, Nankai University. He received his BEng Degree (2010) and MSc Degree (2013) from Zhejiang University, and PhD degree (2016) under the supervision of Prof. Lei Jiang at Beihang University. He has published over 60 peer-review papers in Matter, Adv. Mater., Mater. Horiz. with an H-index of 34. He serves as an Editorial member of Polymers, Chinese Chemical Letters, and an advisory board member of Materials Horizons. His present scientific interests are focused on the design and application of bioinspired fluid-manipulating interfaces.

Published on 04 2023. Downloaded on 31.01.2026 01:32:34.

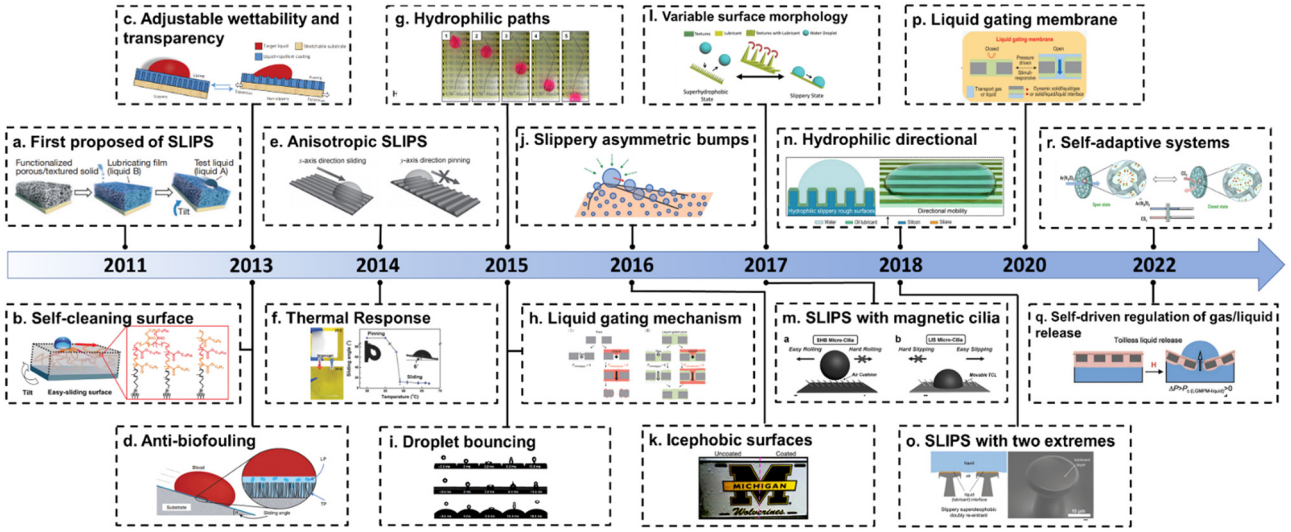

Fig. 1 History of the development of a lubricant infused surface. (a) The first proposed slippery liquid infused porous surface (SLIPS).[11] (b) Self-cleaning surface with the SLIPS.[12] (c) SLIPS with adjustable wettability and transparency.[13] (d) SLIPS resistant to biofouling.[14] (e) SLIPS with anisotropy.[15] (f) SLIPS with thermal responsiveness.[16] (g) SLIPS with hydrophilic path.[17] (h) Liquid gating first proposed.[18] (i) Droplet bounce on different curvatures of lubricants.[19] (j) Slippery asymmetric bumps.[20] (k) Icephobic surfaces with SLIPS.[21] (l) SLIPS with changeable surface morphology.[22] (m) SLIPS with magnetic cilia.[23] (n) Hydrophilic SLIPS with directionality.[24] (o) SLIPS with two extremes.[25] (p) Liquid gating membrane.[26] (q) SLIPS capable of self-driven gas/liquid release regulation.[27] (r) SLIPS with adaptive systems.[28]

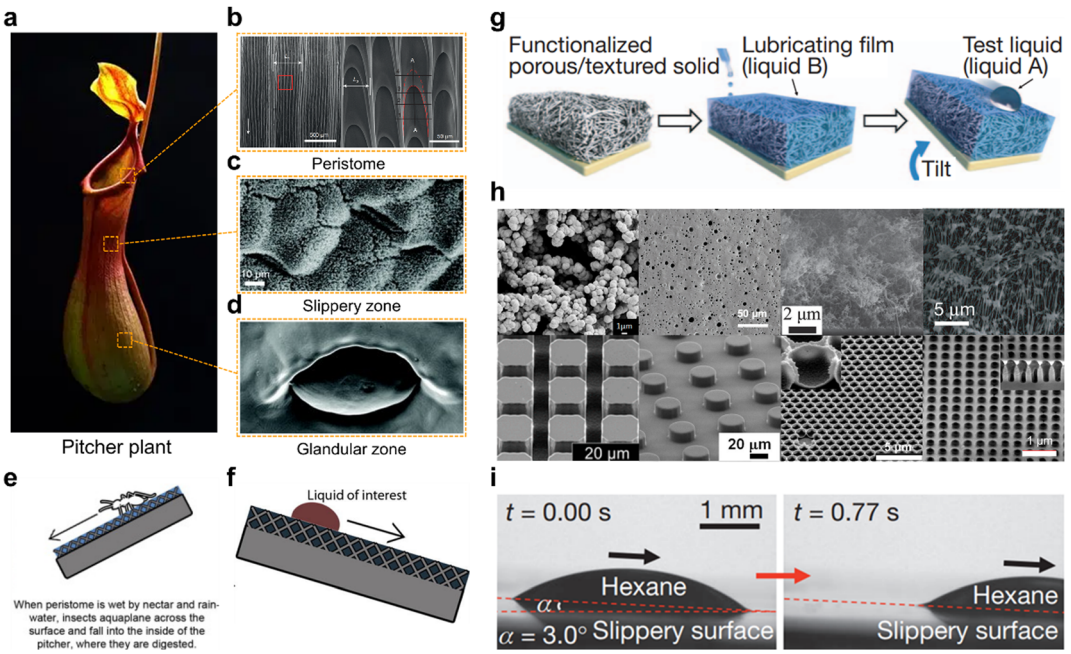

Fig. 2 Pitcher plant and the SLIPS inspired by them. (a) Picture of the Pitcher plant. (b–d) SEM images of the (b) peristome surface,[1] (c) slippery zone surface[10] and (d) glandular zone surface.[10] (e) When the peristome is wet by nectar and rainwater, insects aquaplane across the surface and fall into the inside of the pitcher, where they are digested. (f) The liquid slides off on the inner surface of the pitcher plant. (g) The fabrication process of a typical slippery lubricant infused porous surface.[12] (h) SEM images of representative porous substrates used to fabricate SLIPSs.[11,29–32] (i) A hexane droplet can easily slide on the surface even under a tilt angle of 3.0°.[12]

In general, the preparation of SLIPSs needs to conform to a few simple principles: (a) the infused lubricant fluid should not react with the solid substrate and the repelling fluid. (b) The lubricant liquid and the repelling liquid are immiscible. (c) The solid substrate is preferentially wetted by the lubricant rather than the repelling fluid. (d) The solid substrate should be porous, rough, or swell in the lubricant. The conditions that need to be met to construct a SLIPS can be predicted from the spreading parameters S_{xy} between the phases. Where the first and second subscripts of S_{xy} indicate the spreading phase and

 This journal is © The Royal Society of Chemistry 2023

Published on 04 2023. Downloaded on 31.01.2026 01:32:34.

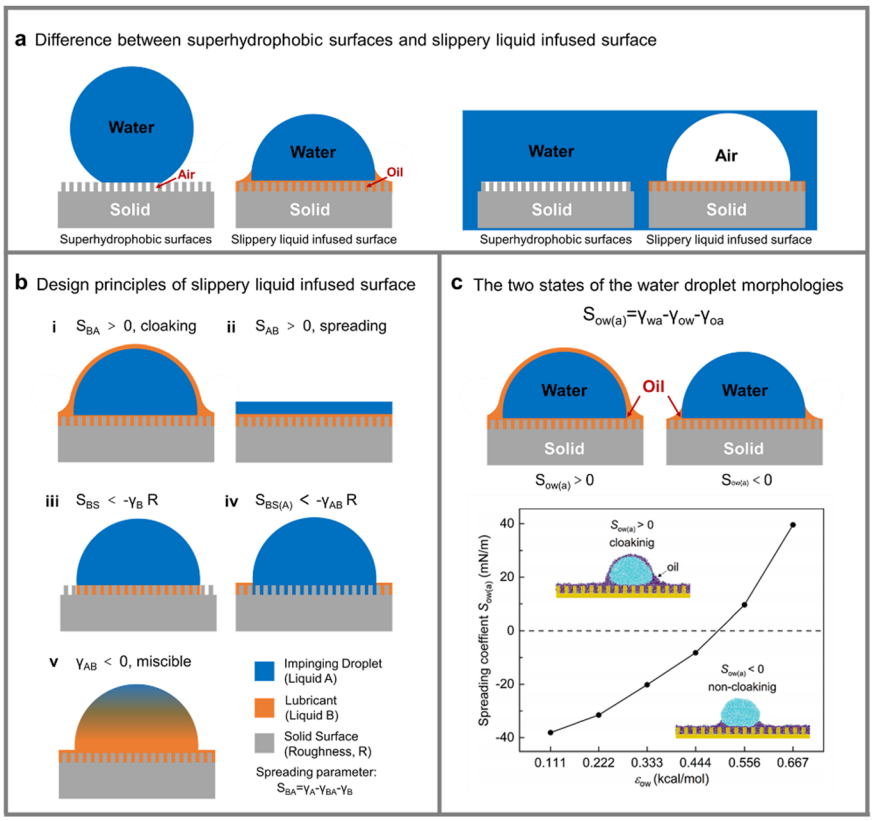

Fig. 3 Contact morphology of SLIPSs with liquid droplets. (a) Difference between superhydrophobic surfaces and slippery liquid infused surfaces. (b) Five failure modes to avoid when designing stable SLIPSs. (c) Two states of the water droplet morphologies.

the reference phase, respectively. The spreading parameters S_{xy} is defined as follows:

$$S_{xy} = \gamma_y - \gamma_{xy} - \gamma_x \quad (1)$$

where γ_x and γ_y are the surface energies of phases x and y with respect to their surroundings and γ_{xy} is the interface energy between phases x and y.

There are several failure modes to avoid when designing stable SLIPSs: (1) $S_{BA} > 0$, the droplet will be covered with a thin layer of lubricant, and the droplet is shown in Fig. 3b(i), which may eventually exhaust the lubricant from the surface when the droplets leave. Therefore, this model is not desirable. (2) $S_{AB} > 0$, the impacted fluid spreads over the SLIPS, forming a liquid film rather than discrete droplets, as shown in Fig. 3b(ii), ultimately leading to the SLIPS failure. (3) $S_{BS} < -\gamma_B R$, the lubricants are less diffusive to solid surfaces than gases and do not spread over roughly structured solid surfaces during operation as shown in Fig. 3b(iii), which could lead to the SLIPS failure. (4) $S_{BS(A)} < -\gamma_{AB} R$, the solid substrate is preferentially spread by the impinging fluid rather than the lubricant, and in the presence of the impinging fluid, the lubricant is not injected into the solid structure as shown in Fig. 3b(iv), that can lead to LIS failure. (5) $\gamma_{AB} < 0$, the impinging fluid and the lubricant are miscible and do not achieve the effect of repelling the impinging fluid, as shown in Fig. 3b(v), resulting in the SLIPS failure.[39] The detailed thermodynamic conditions required for the formation of the stable SLIPS have been described elsewhere, such as Preston *et al.*[39] developed a model to predict the interface surface energy to determine whether any combination of solids and lubricants would repel a given impinging fluid. In 2017, Daniel *et al.* reported a method that can be used to measure the thickness of the lubricant layer called white-light interferometry. The white light reflected from the thin film is collected by an optical fiber with a spot size of about 50 microns and analyzed by a spectrometer. With this method, a thickness in the range of hundreds of nanometers to tens of micrometers can be determined.[40] The relations between diffusion coefficient and droplet configuration were reported in detail by Li *et al.* through molecular simulations.[41] As shown in Fig. 3c, in this system of SLIPS repelling droplets, if $S_{BA} > 0$, the lubricant will cover the droplets; otherwise the lubricant will not encapsulate the droplets (Fig. 4).

The lubricant film thickness on the droplet can be determined by repetitive van der Waals interactions. Therefore, the formula for calculating the lubricant thickness (h) is

$$h = \left(\frac{A}{4\pi S}\right)^{\frac{1}{2}} \quad (2)$$

where A is the Hamaker constant and S is the "spreading coefficient" on the droplet and lubricant. So, when A/S is positive, there will be a stable lubricant film on the droplets.

Published on 04 2023. Downloaded on 31.01.2026 01:32:34.

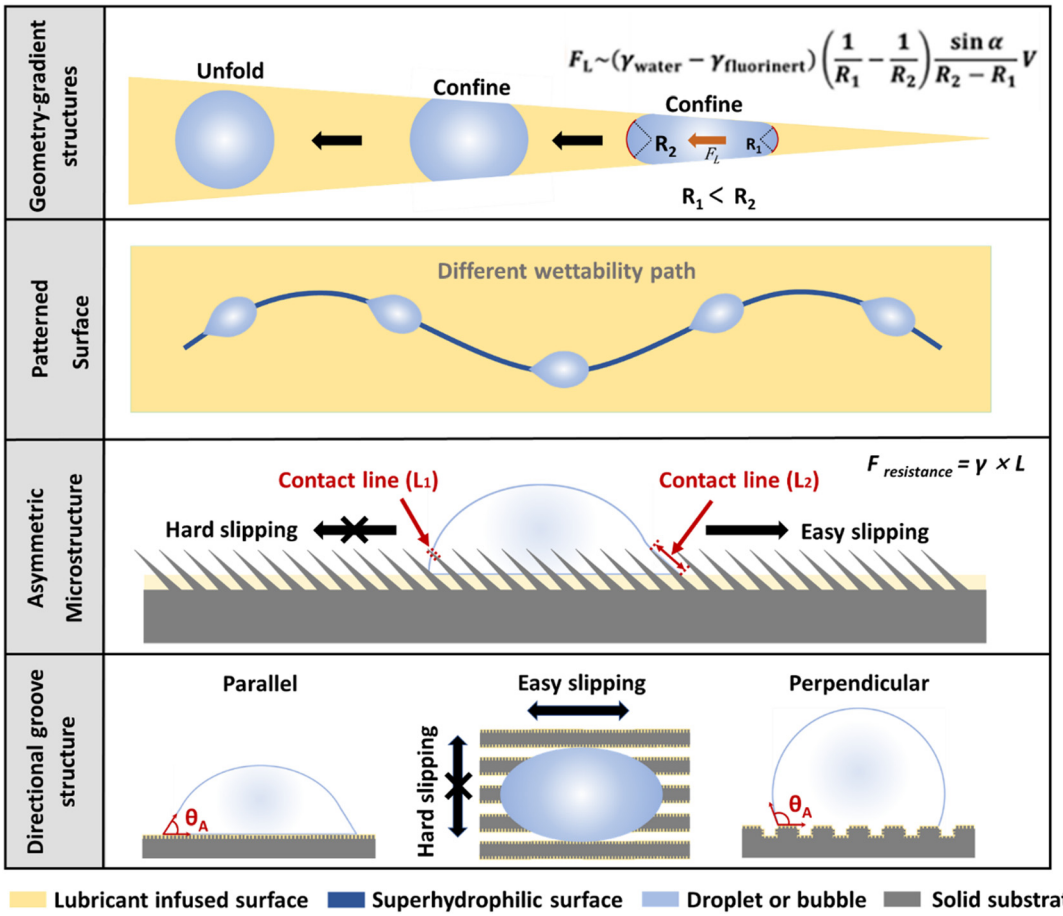

Fig. 4 Several mechanisms of fluid control with SLIPS. From top to bottom, the fluid is controlled by using the Laplace pressure generated by geometry-gradient structures;[45] By combining SLIPS with superhydrophilic surfaces or other surfaces with different wettability to build patterned surfaces to manipulate the fluid motion behavior;[46] By using SLIPSs with an asymmetric surface microstructures to control the fluid forward direction;[23] By combining the directional groove structure with the SLIPS to control the direction of the fluid motion.[47]

In addition, the "cloaking" behavior of SLIPSs will lead to the accelerated loss of lubricant. When low-surface-energy lubricants cover high-surface-energy droplets, the lubricant loses speedily with the loss of droplets, so choosing a lubricant with the proper surface energy is of great importance.[42–44]

2.2 Principles of fluid manipulation with SLIPSs

The special interaction between SLIPSs and fluids such as droplets or bubbles makes it show great promise for fluid manipulation. At this stage, the use of SLIPSs for fluid manipulation is mainly related to four mechanisms.

First, the liquid or bubbles are manipulated by the SLIPS with geometry-gradient structures. For example, on a triangular asymmetric SLIP surface, the droplet or bubble is squeezed by the edge of the SLIPS when it is at the tip site, resulting in a smaller posterior radius of curvature (R_1) and a larger anterior radius of curvature (R_2). Thus, the Laplace pressure on both sides is asymmetric, and the droplet or bubble can achieve a spontaneous and directional transport driven by the asymmetric Laplace pressure. The Laplace pressure difference $\Delta P_{curvature}$ can be expressed by the following equation:

$$\Delta P_{curvature} \sim \left(\frac{1}{R_1} - \frac{1}{R_2}\right)\gamma_{water} \quad (3)$$

where γ_{water} represents the surface tension of water. When the bubble unfolds, R_1 is approximately equal to R_2, resulting in negligible $\Delta P_{curvature}$. Subsequently, the bubble stops moving.[45]

Second, the speed and path of droplets and bubbles can be controlled by introducing a combination of surfaces with different wettability in SLIPSs to form patterns. For example, hydrophilic paths on the SLIPS coated with hydrophobic lubricants can manipulate the paths of water droplets.[46] Geometry-gradient structures and patterned surfaces mainly control bubbles through the difference in wettability in a two-dimensional plane. The difference between them is that geometry-gradient structures use asymmetric Laplace pressure formed by asymmetric patterns to achieve unidirectional fluid transport, while patterned surface simply controls the movement behavior of fluid by using the difference in wettability.

The third is fluid manipulation by SLIPSs with an asymmetric microstructure. For example, SLIPSs with microglia can

 This journal is © The Royal Society of Chemistry 2023

Published on 04 2023. Downloaded on 31.01.2026 01:32:34.

"pierce" the liquid–air interface of a droplet when the droplet or bubble moves toward the tip of the microglia, forming a small circular gas–liquid–solid three-phase contact line. In the opposite direction, the droplet is "held" by the microglia, forming a linear-shaped gas–liquid–solid three-phase contact line. The resistance to droplet sliding (F) can be approximated from the length of the gas–liquid–solid three-phase contact line by the following equation:

$$F = \gamma \times L_C \quad (4)$$

where L_C represents the length of the gas–liquid–solid three-phase contact line. The ratio of its perimeter L_1 to L_2 on both sides is inversely proportional to the resistance to the fluid motion. Therefore, this surface can achieve the unidirectional motion of bubbles or liquids.[23]

Fourth, by combining SLIPSs with a directional groove structure, the unidirectional motion of bubbles or droplets can also be achieved. For example, in a SLIPS with a millimeter-scale groove array, the droplet or bubble has a small contact angle and contact angle hysteresis in the direction parallel to the groove, so the resistance to motion is relatively low. In the direction perpendicular to the groove, the droplet or bubble has a large contact angle and contact angle hysteresis, so it is difficult to move in the vertical direction.[47] These two principles of asymmetric microstructure and directional groove structure can manipulate the fluid through a three-dimensional asymmetric structure. The difference is that the asymmetric microstructure is designed from a microscopic point of view, while the directional groove structure combines SLIPS with a macroscopic asymmetric structure. Considering the fluid manipulation, the asymmetric microstructure is able to realize a unidirectional fluid motion as a fluidic diode, whereas the microgroove structure usually shows a directional fluid motion in one dimension.

2.3 Preparation approach

A number of preparation methods have been developed for SLIPSs to date. The SLIPS consists of two main components, a porous or rough solid substrate, and an upper lubricant layer. In 2012, Aizenberg and co-workers reported a method for the preparation of SLIPSs on aluminium,[48] copper,[49] and steel[50] surfaces by electrochemical deposition, respectively. The corrosion of metal electrodes is used to create porous surfaces (Fig. 5a), which are hydrophobically treated and then injected with lubricants to obtain a stable SLIPS. In 2013, Ryan *et al.* reported a silane self-assembly method to prepare SLIPSs by vapor depositing (Fig. 5d) a highly self-assembling silane onto a corroded metal surface to obtain a superhydrophobic surface and then injecting a lubricant to obtain stable a SLIPS.[50] In 2014, Qi and co-workers prepared SLIPSs on a glass surface by dropping a highly self-assembled low-molecular polymer solution onto a glass surface, drying it to obtain a superhydrophobic surface, and then infusing a lubricant (Fig. 5c).[50] This layer-by-layer method of preparing superhydrophobic surfaces followed by SLIPSs has become a very common method of SLIPS preparation. However, some more simple and highly effective novelty methods of SLIPS preparation still need to be introduced. In 2017, Feng Chen and his colleagues introduced the femtosecond laser into the SLIPS preparation process,[51,52] *i.e.*, the preparation of SLIPS on PA6 substrate surfaces by femtosecond laser ablation, fluoro silane substrate modification and lubricant infusion (Fig. 5b), and they later reported that this method is also applicable to polyethylene terephthalate (PET) substrate surfaces.[26] Compared to electrochemical deposition methods, SLIPSs prepared in this way are more self-healing and have a smaller droplet roll angle. George M. Whitesides and his group have reported on a paper-based SLIPS that ingeniously combines the foldability of paper with the liquid-repelling properties of the SLIPS, which makes the SLIPS more functional.[53] The template-assisted molding method is also an effective means of preparing SLIPS, as shown in Fig. 5e.[54] This method is applicable to SLIPSs with various polymers (*e.g.*, PDMS) as solid substrates. Similarly, obtaining porous polymers by introducing other phases insoluble in polymer solvents into the polymerisation process is an effective

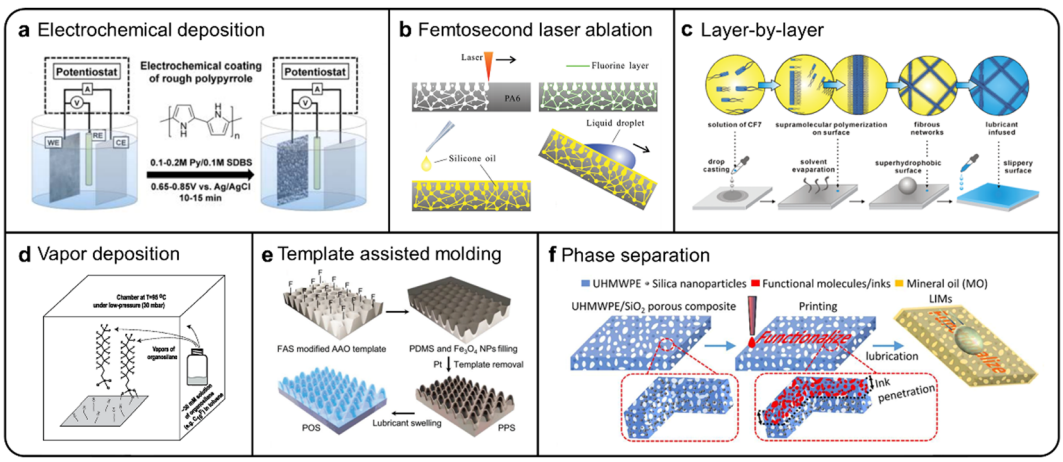

Fig. 5 Schematic diagram of different preparation methods of the SLIPS. (a) Electrochemical deposition process.[48] (b) Femtosecond laser ablation.[25] (c) Layer-by-layer deposition.[50] (d) Vapor deposition process.[53] (e) Template assisted molding.[54] (f) Phase separation.[55]

Published on 04 2023. Downloaded on 31.01.2026 01:32:34.

Table 1 Typical examples of SLIPSs

Substrate materials	Fabrication process	Infused lubricants	Manipulating liquids	Contact angle (deg.)	Contact angle hysteresis (deg.)	Sliding angle (deg.)	Ref.
Aluminum sheets	Electrochemical deposition	Perfluoroalkylether	Water	116 ± 3	2 ± 1		48
Steel plates	Electrochemical deposition	DuPont Krytox GPL-K103	Water	124 ± 1	1.4 ± 0.5	3.0 ± 0.3	50
Paper	Chemical vapor deposition	DuPont Krytox GPL-K105	Water	>140	<20		53
Oxygen-free Cu tubes	Alkali corrosion and vapor deposition	TFTS	Water	≈110	3		50
PA6	Femtosecond laser ablation	Silicone oil	Water			<3	25
			Hexadecane			<3	
PET	Femtosecond laser ablation	Silicone oil	Water		27.5 ± 0.1	0.6	26
APTES, D_4^H/Si substrate	Chemical vapor deposition and spin-coating	[EMI] [TFSI]	Water	51.1 ± 1.0	1.4 ± 0.4	3.0 ± 0.7	65
			Diiodomethane	52.4 ± 1.2	2.5 ± 1.4	2.3 ± 0.6	
			Liodobenzene	27.7 ± 1.3	2.2 ± 1.0	1.3 ± 0.5	
			N-Hexadecane	33.0 ± 0.8	1.8 ± 0.8	2.0 ± 1.1	
			N-Tetradecane	28.7 ± 0.7	1.1 ± 0.8	2.3 ± 1.6	
			N-Dodecane	24.4 ± 0.3	1.6 ± 0.6	3.8 ± 2.2	
			N-Decane	17.0 ± 1.7	1.6 ± 2.2	3.7 ± 1.2	
PS/glass	Spin coating, freeze-drying, immersion	Paraffin wax, liquid paraffin	Water	107.6 ± 2.0		33.2 ± 2.8	66
			Glycerol	97.5 ± 2.1		17.6 ± 2.5	
			Formamide	92.1 ± 1.6		18.9 ± 2.1	
			EG	81.8 ± 1.7		21.4 ± 2.3	
			DMSO	68.0 ± 1.9		24.7 ± 2.0	
			[OMI] [BF4]	60.7 ± 2.2		27.2 ± 2.1	
CF7/glass	Supramolecular self-assembly, drop-casting	Fluorinert FC-70	Water	27.2 ± 1.1	9.8	<10	59
			4% CTAB	28.3 ± 2.5	8	<10	
			4% SDS	23.4 ± 3.1	0.5	<10	
			Human serum	29.1 ± 1.7	9	<10	
PFDA, TTT, PETMP, BME, PGMEA, PET	Roll-to-roll nanoimprinting	Krytox PFPE lubricant	Water	114		<10	67
			Glycerol	103		<10	
			EG	93		<10	
			Hexadecane	70		<10	
UHMWPE/SiO_2	Thermally induced phase separation	Mineral oil	Water	92 ± 2.7	2.4 ± 1.5	<10	
bPEI, Nafion/glass, Si, PET	Layer-by-layer	Krytox 100	Water	~110		~1.5	68
			PBS	~111		~2.5	
			Decane	~55		~1	
			Methanol	~65		~9	
			Acetone	~56		~12	
			Toluene	~63		~3	
Zinc	Solution etching, grafting to method	Ungrafted silicone oil	Water	89.5		2.4	54
			Oleic acid	31		2.8	
ZnO NRs, FAS-13/ wood	Dip-coating, drop-casting	Krytox 100	Water	~130/ ~86		<15	69
			EG	~88/~62		<17	
Fe_3O_4 NPs, Sylgard 184	Solvothermal synthesis, template assisted molding, immersion	Silicone oil	Water	~107		~2	70
			Glycerol	~96		~2	
			EG	~86		~2	
			Propylene glycol	~72		<2	
			Ethanol	~22		<2	
PFOEA, PFHEA, PFPE-DMA/PDMS	Bulk polymerization	Krytox 100, FC-70	Water	~121	15	<10	54
			Hexadecane	~6		<10	
PhTEOS, TMOS/glass PET	Spin-coating, sol-gel, drop-casting	Decyltrimethoxysilane	Water	77.9 ± 1.3	1.75 ± 0.3	0.5 ± 0.1	71
PGMA-*g*-PDMS, DGEBA, Jeffamine®	Solution self-assembly, drop-casting	Silicone oil	Water	108 ± 1	<1	<1	72
			Hexadecane	16 ± 1	<1	1 ± 1	
			Dodecane	14 ± 1	<1	1 ± 1	
			Decane	10 ± 1	<1	<1	
			Octane	4.8 ± 0.4	<1	2 ± 1	

means of preparing SLIPS solid substrates (Fig. 5f).[55] In addition, film swelling,[56] lubricant-substrate bonding,[57] and 3D printing,[25,58] *etc.* are some simple and practical methods for the preparation of SLIPSs. Due to space limitations, these methods will not be described in detail, and preparation methods of some typical SLIPSs are compared and contrasted in Table 1.

 This journal is © The Royal Society of Chemistry 2023

Published on 04 2023. Downloaded on 31.01.2026 01:32:34.

2.4 Stability of SLIPSs

As the old Chinese saying goes, you can never cleave water flows with a knife. Compared to other liquid-repellent surfaces, the mobile lubricant layer of the SLIPS can repel another immiscible liquid, endowing it with a self-healing characteristic. The SLIPS has a flowable lubricant layer that spontaneously fills and repairs mechanically damaged areas, enabling a self-healing process. In 2011, Wong *et al.* demonstrated that ~50 μm damage on SLIPSs could be self-repaired without affecting the flow of the lubricant.[11] In addition, self-healing gels with specific polymer networks are considered as effective liquid absorbers as well as suitable substrates for smooth surfaces.[12] In 2013, a colloidal template nanoporous surface structure for the SLIPS was reported by Vogel *et al.*[30] This SLIPS is extremely well tolerated in terms of mechanical stability, which is attributed to the honeycomb hexagonal structure (Fig. 6a), while the self-healing fluid repellency is based on lubricant refilling. In 2014, Wei *et al.* demonstrated that a slippery surface built on a self-assembled three-dimensional fiber network could achieve a high-speed self-healing process (<1 min) of the substrate material.[59] In contrast, a superhydrophobic surface made of similar materials can only self-heal within 20 min even under microwave treatment. The results suggest that liquid infusion should enhance the mobility of polymer chains and accelerate the self-healing process. In 2014, Howell *et al.* introduced a 3D "vascular system" into PDMS as a lubricant reservoir to supplement the lubricant.[60] In 2015, Cui *et al.* reported a SLIPS with a self-regulating, self-reporting secretion system.[61] The authors demonstrated that dynamic fluid exchange between the compartment, matrix, and surface layer allows for repetitive, responsive self-lubrication of the surface layer and cooperative healing of the matrix. Depletion of surface fluids or damage to local material leads to the self-regulated secretion of stored fluids through dynamic feedbacks between polymer cross-linking, droplet shrinkage, and fluid transport that can be read off by changes in the optical transparency of the system (Fig. 6f). In 2018, Zhao *et al.* devised a simple synthetic strategy to develop soft polymer coatings with adaptive friction reduction, wear and self-cleaning properties in solid environments by simulating the passage of earthworms through a viscous soil pattern.[62] The coating has a textured surface with

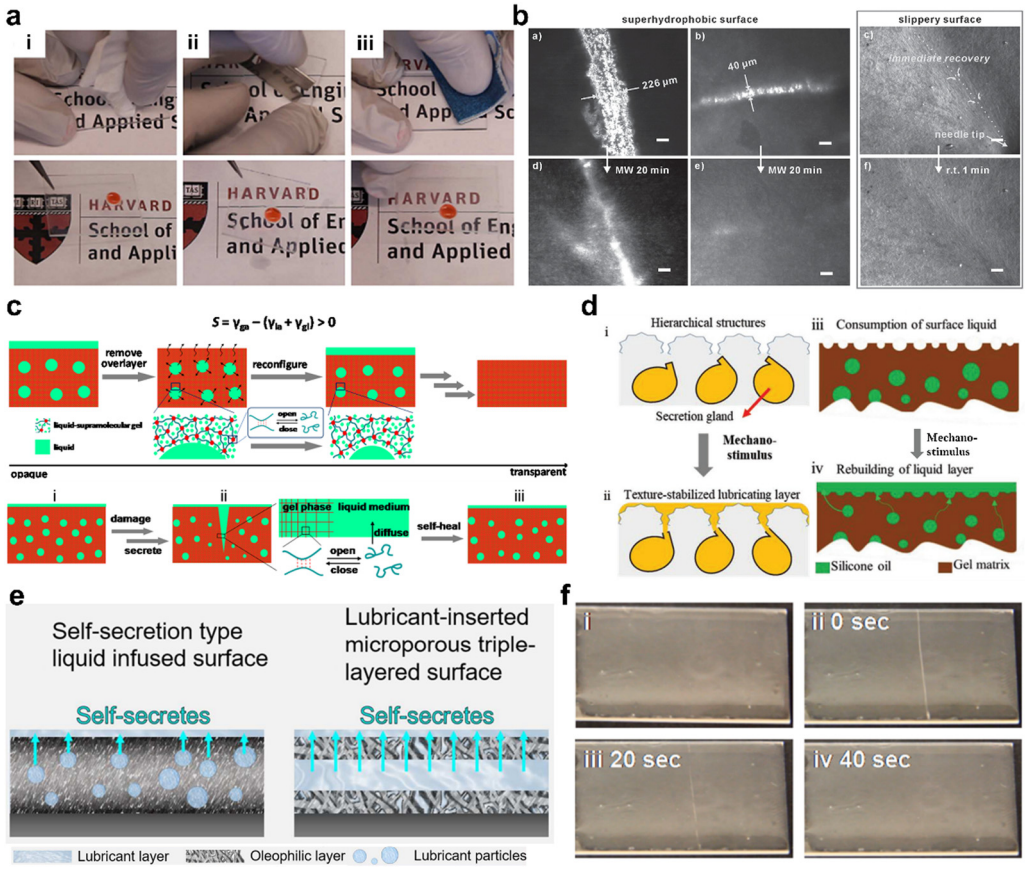

Fig. 6 Self-healing designs of SLIPS. (a) Slippery surface with outstanding damage tolerance. After mechanical wiping (i), scratching with a blade (ii) and sandpaper (iii), the slippery nature of the surface was still preserved.[11] (b) The self-repairing property of the slippery surface was significantly enhanced as compared to self-healable superhydrophobic surfaces. Based on similar materials, the slippery surface shows an order of magnitude higher rate of self-healing (1 min) than that of the superhydrophobic surface (20 min).[59] (c) Schematic of the self-regulated, liquid secretion system and secretion-mediated response to polymer damage.[61] (d) Earthworm-inspired stimulus-responsive gel membrane.[62] (e) Self-secretion type LIS and lubricant-inserted (sandwiched) microporous triple-layered surface.[63] (f) Optical images of PDMS-based SLIPS films before damage and after damage.[61]

Published on 04 2023. Downloaded on 31.01.2026 01:32:34.

a fixed oil layer and droplet-embedded blocks. The lubricant stored in the droplets can be specifically and rapidly released in response to external mechanical stimuli, restoring the oil layer and thus maintaining a slippery functional surface. Similarly, Tenjimbayashi *et al.* introduced a lubricant insertion (sandwich) into the microporous trilaminar surface (limit) to prevent sudden loss of the lubricant.[63] The lubricant of the sandwich layer gradually self-secreted to the surface and remained stable for a long time, even in water. This SLIPS prevented corrosion of the iron plate for at least 45 days, which is much better than the conventional SLIPS coating. In 2021, Sun *et al.* designed a lubricant-injected layered porous surface with an anti-opaline nanoporous structured outer surface layer with liquid-repellency properties for liquids with different surface tensions (22.3 mN m^{-1} to 72.8 mN m^{-1}) and good lubricant self-refill capability for stable droplet manipulation.[64]

3 Applications

SLIPSs are somewhat similar to superhydrophobic surfaces in terms of application direction due to the liquid repellency of the lubricant on the surface but differs significantly from superhydrophobic surfaces due to the molecular smoothness, self-healing, and incompressibility of the lubricant. Nowadays, SLIPSs are used for droplet and bubble manipulation, vapor condensation, fog collection, anti-icing, anti-biofouling, self-healable/damage tolerant surfaces, and liquid-gating.

3.1 Droplet manipulation without external stimuli

The manipulation of the behavior of liquids offers great opportunities for the development of microfluidic devices, microreactors, and intelligent fluid manipulation systems.[73] Scientists have recently discovered that SLIPS materials inspired by the pitcher plant are an effective surface for fluid manipulation.[74,75] Combining SLIPSs with patterns that differ in wettability as well as shape gradients enable manipulation of the behavior of droplets. In 2015, Manna *et al.* reported on a SLIPS coating formed by a layer-by-layer deposition method.[46] They demonstrate that the sliding trajectory of the droplets is controlled when guided by the hydrophilic path of the slippery surface (Fig. 7a). In 2014, Zhang *et al.* proposed an anisotropic micro-grooved organogel slippery surface consisting of polybutyl methacrylate-lauryl methacrylate and silicone oil, which successfully introduced anisotropy into SLIPS, showing good droplet manipulation.[15] In 2018, Pavel A. Levkin *et al.* demonstrated that by choosing the appropriate chemical surface patterning, liquid–liquid displacement could be spatially controlled for a wide range of lubricant-intruding liquid pairs.[76] In 2018, Xianming Dai and co-workers designed a SLIPS with a directional texture and demonstrated that the combination of this directional surface structure and the lubricant facilitated the removal of droplets.[24] There is no difference in mechanism between the SLIPS with a directional texture designed by Dai *et al.* and anisotropic microgroove textured SLIPSs proposed by Zhang *et al.* Both of them use directional grooves to promote the directional flow of droplets. However, the lubricant on the

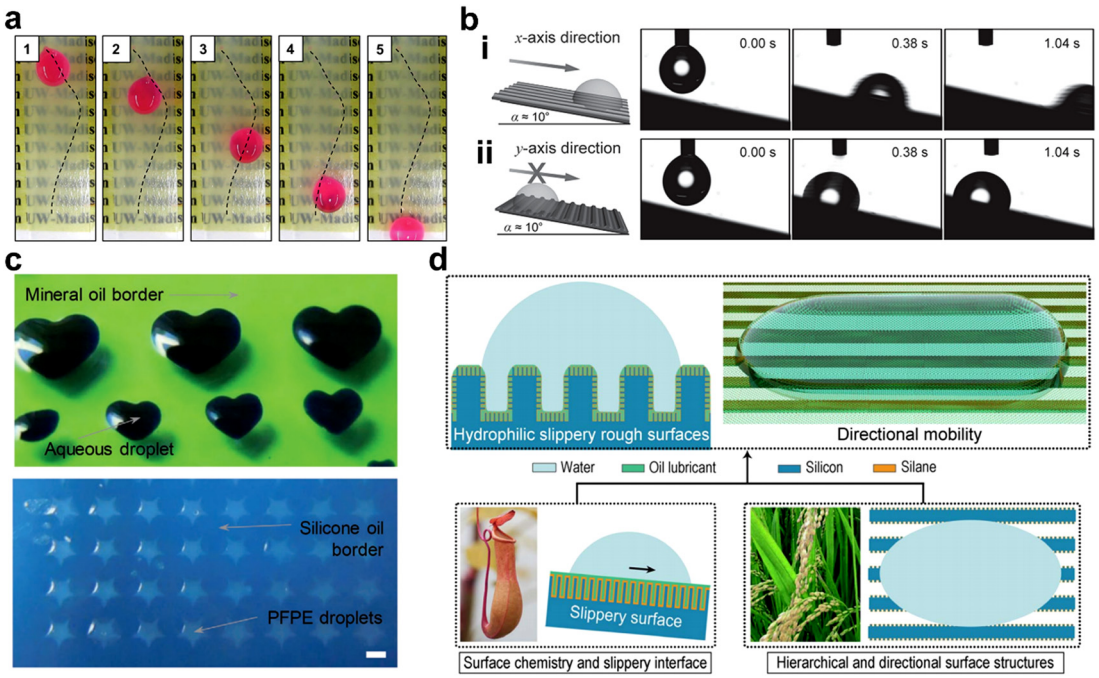

Fig. 7 Droplet manipulation by SLIPSs with patterns and asymmetric structures. (a) Patterned slippery surface can regulate the sliding pathway of droplets through a selectively hydrophilic modification.[46] (b) Slippery surfaces with a grooved structure achieved an anisotropic droplet manipulation.[15] (c) Images of patterned SLIPSs with alternative lubricant system including water droplets surrounded by a mineral oil lubricant and perfluoropolyether droplets surrounded by a silicone oil background.[76] (d) SLIPSs with a directional texture, this structure promotes the coalescence and removal of droplets.[24]

 This journal is © The Royal Society of Chemistry 2023

Published on 04 2023. Downloaded on 31.01.2026 01:32:34.

SLIPS with a directional texture designed by Dai *et al.* is hydrophilic and can be used to promote droplet nucleation, while the lubricant of anisotropic microgroove textured SLIPS proposed by Zhang *et al.* is hydrophobic in order to promote the rapid directional movement of droplets. In 2019, Li *et al.* present in this paper an integrated lattice with an integrated mesh with orthogonal anisotropic slippery tracks (IMOAS) that can achieve similar unidirectional droplet penetration using a unique mechanism. The unidirectional droplet penetration can be easily switched by 90° rotation of the IMOAS, showing highly controllable liquid manipulation.[77]

3.2 Droplet manipulation with external stimuli

The introduction of smart responsiveness into the SLIPS has been shown to be an effective way of achieving intelligent manipulation of droplets. In 2013, Yao *et al.* reported an adaptive SLIPS with a flexible structure based on porous polytetrafluoroethylene films.[13] This SLIPS has a property that when the substrate is bent, the substrate area increases, the lubricant layer becomes thinner and various droplets will pin on its surface. When the substrate is relaxed, the substrate area decreases, the lubricant layer becomes thicker and droplets slide easily over its surface. This work creates a new way of controlling droplet sliding with mechanical methods of stretching and relaxing. In 2014, Jianjun Wang *et al.* prepared an organogel capable of converting hydroviscosity under thermal stimulation by exploiting the phase change properties of n-paraffin.[16] At temperatures below the paraffin melting point, the micro-phase separation of paraffin gives rise to a Wenzel state, which shows high viscosity to water droplets. Whereas at temperatures above the paraffin melting point, organogel surfaces wetted with liquid paraffin and homogeneous organogels and water droplets form an ALLS system in which the water droplets show a low viscosity sliding state. Here, the conversion of low droplet adhesion to high adhesion is achieved simply by temperature. In 2014, Hao *et al.* demonstrated a new paradigm of electrical wetting on liquid-infused thin films (EWOLF) that allows for full reversibility and controlled droplet oscillation suppression, enabling fast optical imaging.[78] In 2017, Moyuan Cao *et al.* prepared an anisotropic SLIPS by infusing lubricant into magnetic microglia, which achieved excellent magnetic response for droplet manipulation.[23] As shown in Fig. 8c, when the droplet moves in the direction opposite to the tilting direction of the cilia, it can slide smoothly, while when it is in line with the tilting direction of the cilia, the droplet will pin on its surface. The behavior of the droplet can be manipulated

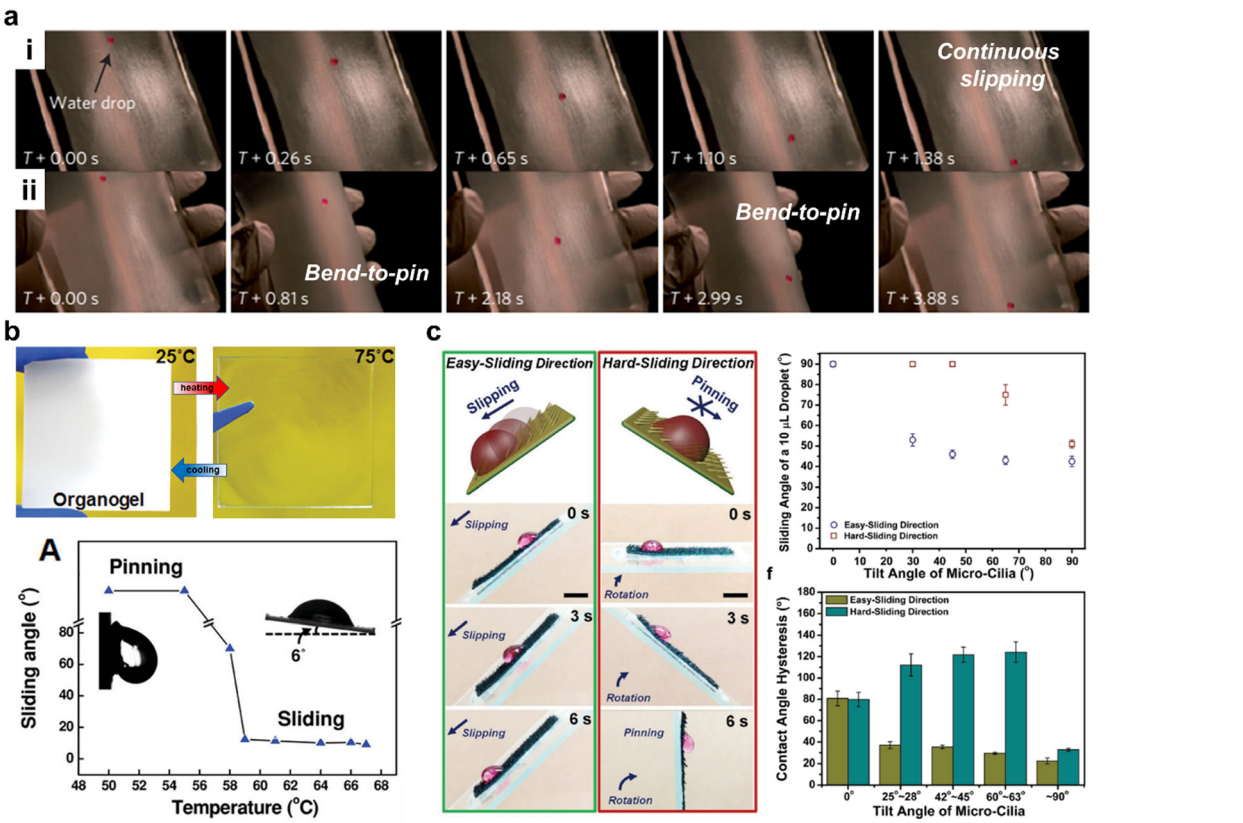

Fig. 8 Droplet manipulation by stimulating responsive SLIPSs. (a) The adaptive slippery surface exhibited an external force controlled droplet manipulation. The droplet can slide on the relaxed surface, and stop slipping when the substrate is bent, *viz.* a bend-to-pin process.[13] (b) A thermally responsive SLIPS prepared using *n*-paraffin wax showed a droplet rolling angle of less than 6° when the temperature was below the melting point of paraffin wax and a large droplet adhesion when the temperature was above the melting point of paraffin wax.[16] (c) SLIPSs with asymmetric ferromagnetic microcilia. Droplets more easily move against the direction of the ferromagnetic microcilia and less easily move in the direction of the compliant ferromagnetic microcilia, scale bar represents 5 mm.[23]

Published on 04 2023. Downloaded on 31.01.2026 01:32:34.

by controlling the tilting direction of the cilia through a magnetic field. In 2022, Cai *et al.* reported a tridirectionally anisotropic slippery surface with periodically stepped microgrooves for programmable droplet transport.[79]

3.3 Underwater bubble manipulation

Manipulation of bubbles in the aqueous environment has become a valuable approach for the improvement of current systems, such as enzyme sensors,[80–82] electrolytic water,[83,84] and heterogeneous catalysis.[85–87] However, the means to manipulate bubbles in aqueous environments are now very limited. Superhydrophobic surfaces as effective gas carriers facilitate multiphase reactions containing gases.[88–91] Nevertheless, superhydrophobic properties will be ineffective in humid, petroleum, and high-pressure environments due to the suppression or deterioration of air among micro/nanostructures. When SHB surfaces are underwater for a long time, there is an irreversible Cassie to Wenzel state transition on its surface, *i.e.*, a gradual replacement of the gas by water in the micro-nano structure, which will make the SHB surface no longer attractive to the gas and lose the ability to manipulate bubbles.

As a new functional surface, SLIPS surfaces excel in the manipulation of underwater bubbles due to the hard-to-replace liquid lubricant on its surface and its incompressible nature. In 2017, Yu *et al.* proved that SLIPS is suitable for manipulating bubbles underwater.[92] They prepared paper-based SLIPS by dip-coating process, with silicone oil as a lubricant. This SLIPS has good bubble adhesion and enables a series of bubble manipulation processes, such as track changes during continuous bubble transport using three exit bifurcated SLIPS tracks (Fig. 9a). The same year, Tiantian Kong and co-workers designed a SLIPS track that allows for rapid collection and transport of gases underwater as shown in Fig. 8g.[93] In 2018, Chunhui Zhang *et al.* designed a SLIPS with an asymmetric structure that deforms the bubble to generate a driving force for the directional motion of the bubble, as shown in Fig. 9c.[45] In 2020, Liu *et al.* designed a fluoro silicone fluids-infused shaped slippery gradient surface that enables bubble manipulation in harsh environments.[94] In 2021, Kai Zhuang reported a three-dimensional topology of SLIPS, which realized the directional transport of underwater bubbles using curved arrays and wedge arrays in combination with SLIPSs.[47] Smart response of SLIPSs

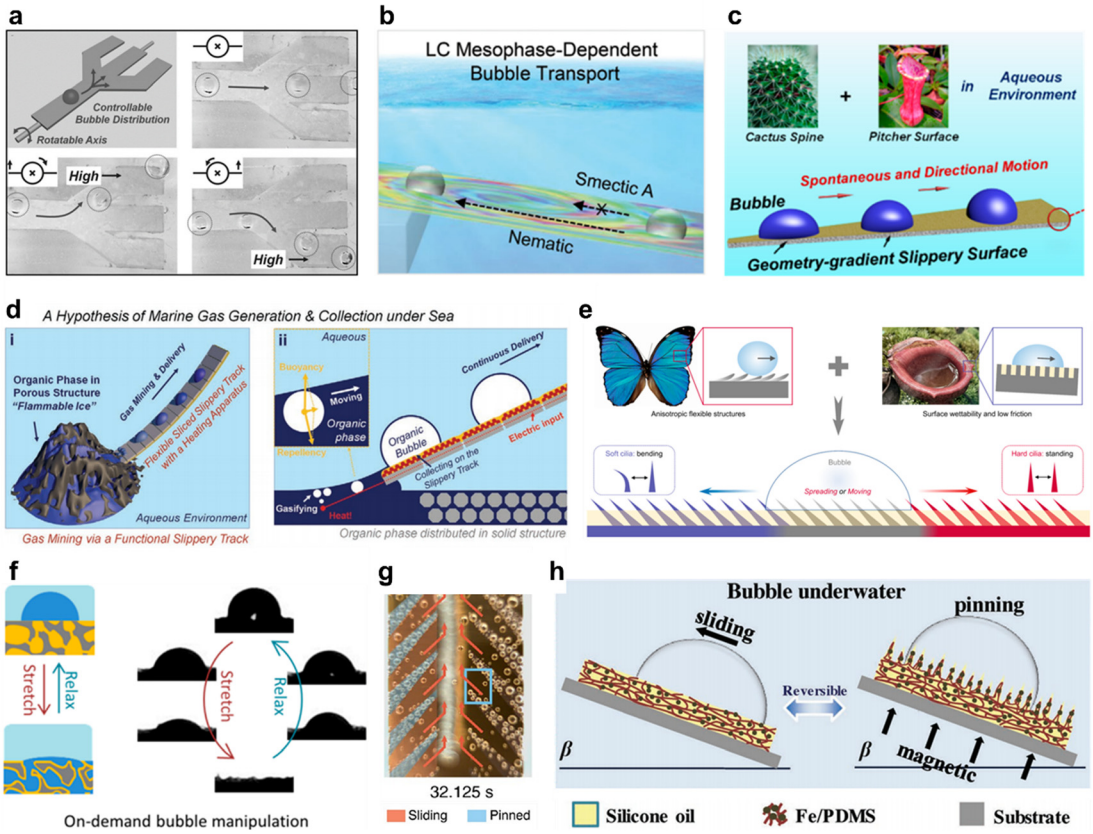

Fig. 9 Air bubble manipulation by SLIPSs. (a) Change tracks during continuous bubble transport by using a paper-based SLIPS track with three exit bifurcations.[92] (b) Thermally responsive SLIPSs prepared with thermally sensitive liquid crystals.[95] (c) SLIPSs with an asymmetric structure that deforms the bubble to generate a driving force for the directional motion of the bubble.[45] (d) Piecewise stitching of SLIPS tracks enables *in situ* bubble generation, capture and transport processes.[98] (e) SLIPSs with asymmetric cilia allow for unidirectional transmission of bubbles. On soft cilia, bubbles tend to spread or move along the tilt direction of cilia, due to its easy bending property. While, on hard cilia, a bubble prefers to spread or move against the tilt direction of cilia because of its standing character.[100] (f) Bubble manipulation *via* a biomimetic elastic liquid-infused material with a responsive injection of liquid or gas.[99] (g) SLIPSs prepared on copper surfaces for rapid collection and transport of gases underwater.[93] (h) Magnetically responsive amphibious hydrogel that enables bubble manipulation.[96]

 This journal is © The Royal Society of Chemistry 2023

Published on 04 2023. Downloaded on 31.01.2026 01:32:34.

also enables intelligent control of underwater bubbles. In 2022, Adil Majeed Rather and co-workers reported a thermally responsive SLIPS that enables programmable manipulation of underwater bubbles (Fig. 9b) by introducing thermotropic liquid crystals into this SLIPS.[95] Heng *et al.* developed an amphibious slippery gel surface on which magnetically controlled motion of air and air bubbles was achieved. Magnetically controlled motion of air bubbles underwater was realized.[96] Chen *et al.* reported an intelligent manipulation of underwater bubbles using magnetic particles in combination with SLIPSs.[97] In 2021, Wang *et al.* designed a piecewise spliced SLIPS track with a drawbridge-like structure that combines flexibility and resilience, enabling a variety of complex underwater bubble manipulations such as bubble merging, movement speed, and motion/pinning through deformation and stretching/relaxation of the track.[98] Xi Yao and co-works proposed a biomimetic elastic liquid-infused material to mimic the characteristics and functions of the alveolar system in manipulating air bubbles under underwater conditions; this elastic liquid-infused material implements a conceptual strategy for bubble manipulation through reversible adaptation of the injected liquid–gas interface to substrate response deformation as shown in Fig. 9f.[99]

3.4 Droplet energy harvesting

With the increase of the global energy crisis, low-cost and sustainable energy acquisition methods become more and more important. In recent years, some water energy collection technologies that rely on the generation and transfer of interface charges have attracted more and more scholars' attention. In 2015, Hao *et al.* explored the bouncing behavior of droplets on hydrophobic SLIPS and proved that the bouncing behavior of droplets is related to the weber number, thickness and viscosity of lubricant film.[19] This lays a foundation for further utilization and transformation of droplet energy. Fig. 10a shows a typical droplet-based electricity generator (DEG), which consists of a top electrode, a dielectric layer (PTFE) and a bottom electrode.[101] Power generation depends on the hydrodynamic interaction and charge transfer among the impinging droplets, hydrophobic dielectric materials and electrodes. In 2019, Xu *et al.* combined SLIPS with triboelectric nanogenerators (TENGs) and proposed a novel SLIPS-TENG, which can effectively convert the kinetic energy or wave power of environmental water droplets into electric energy.[102] As shown in Fig. 10c, the generated charges from an impinging water droplet on SLIPS-TENG are measured to be ~ 3 nC g^{-1}. In 2022, Song *et al.* optimized the water energy collection system by using lubricant armor, which made the hydro-generator to obtain better stability, electrical performance and expandability.[102] This promotes the practical application of a water drop generator. Wang *et al.* proposed light-induced charged slippery surfaces, which can have both advantages of a solid and a lubricant.[103] As this surface has the ability of light-induced charge generation, under the action of Marangoni force (FM) generated by temperature gradient and dielectrophoretic force (Fe) generated by an asymmetric electric field, it can realize rapid, long-distance, anti-gravity and directional droplet manipulation.

3.5 Vapor condensation

Vapor condensation is a ubiquitous process in both industry and daily life, such as distillation processes, desalination, fog collection, power generation, and refrigerators. The condensation process is generally divided into dropwise condensation and filmwise condensation. Once a liquid film is formed on the wall surface, the condensation of vapor can only take place on the surface of the liquid film, *i.e.*, the latent heat released during the condensation of vapor must pass through the liquid film before it can be transferred to the cold wall surface. The liquid film relies on heat conduction, and the thermal conductivity of the fluid is usually small, making the film the main thermal barrier to condensation. In dropwise condensation,

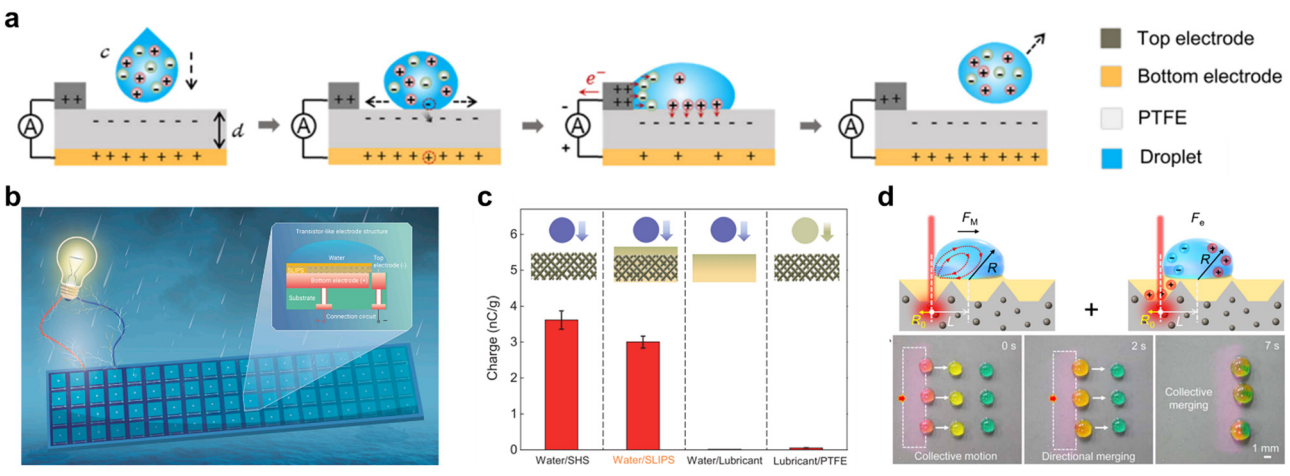

Fig. 10 Droplet energy harvesting by SLIPS. (a) Schematic diagram of the process of converting the kinetic energy of water droplets into electric energy.[101] (b) Lubricant-armored transistor-like electricity generator.[102] (c) Compare the charges obtained by the droplets hitting various interfaces, including water/SHS, water/slide, water/lubricant and lubricant/PTFE interfaces. The charge generated on SHS and slider is far greater than that generated at the interface of water/lubricant and lubricant/PTFE.[104] (d) Light-induced charged slippery surfaces.[103]

Published on 04 2023. Downloaded on 31.01.2026 01:32:34.

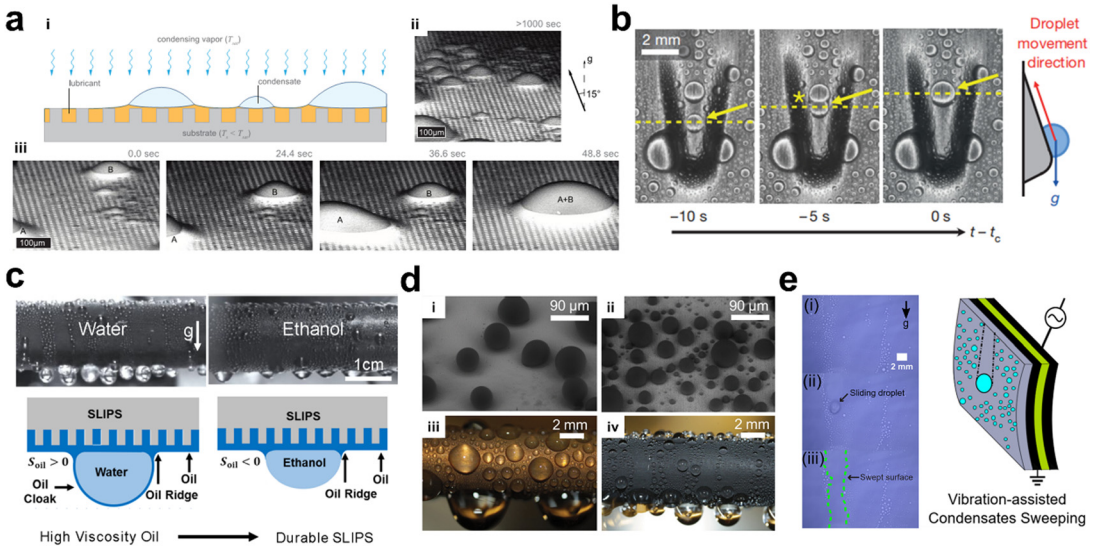

Fig. 11 Promoting vapor condensation with SLIPS. (a) The vapor condensing process of slippery surfaces. (i) The schematic diagram of vapor condensation on a slippery surface, and (ii) the final droplet distribution after 1000 seconds condensation. (iii) The growth and coalescence of condensate droplets were observed by environmental scanning electron microscope (ESEM), indicating the tiny droplets have high mobility on such surfaces.[105] (b) SLIPSs with asymmetric protrusions promote droplet coalescence and removal.[107] (c) The morphology of droplets on SLIPSs as a lubricant is lost.[111] (d) The comparison of vapor condensation between (i & iii) the superhydrophobic surface and (ii & iv) the slippery surface.[50] (e) Vibrating SLIPS to promote droplet removal.[110]

most of the wall surface area is directly exposed to the vapor and is available for vapor condensation. Since there is no liquid film to impede the heat flow, the dropwise condensation heat transfer coefficient can be several times or even a dozen times higher than that of filmwise condensation. The SLIPS is considered a potential substrate for high-performing vapor condensation as a stable liquid rejection surface capable of drop condensation. In 2012, Anand *et al.* reported that the SLIPS facilitates the vapor condensation process. During the condensation process, the lubricant layer encapsulates the condensed droplet, which limits the growth of the droplet and makes it easier for it to slip away on the surface.[105] The authors further investigated the detailed mechanism of the droplet formation and growth process on SLIPS.[106] A mechanism was found for condensing droplets to nucleate at the liquid–air interface and then immerse in the stealth liquid. In 2013, Xiao *et al.* proved that SLIPS showed a 100% improvement in heat transfer efficiency compared to typical superhydrophobic surfaces during droplet condensation.[50] As shown in Fig. 11d, the ESEM images showed that the condensate droplet on the superhydrophobic surface (i) is larger than that on the slippery surface (iii). Therefore, the droplet departure volume of the slippery surface is relatively small (ii & iv), promoting a higher efficiency of heat transfer. Later, Park *et al.* introduced asymmetric topography to SLIPSs in 2016.[107] This reduced the time for droplet growth during condensation and increased the transport rate. As reported by Adera *et al.* in 2020, the lubricant of SLIPS is lost with the vapor condensation process, and if the substrate roughness of SLIPS is changed to the nanoscale, the lifetime of SLIPS during vapor condensation is increased by a factor of 2–3.[108] After 10 hours of continuous vapor condensation at environmental pressure, 23 °C, and 60% relative humidity, nearly half of the lubricant remained on the surface. In 2018, Preston *et al.* demonstrated an increase in heat transfer efficiency of approximately 450% for SLIPSs compared to uncoated condensing surfaces.[109] In 2020, Miljkovic *et al.* reported a vibrating SLIPS that allows a 39% reduction in the droplet leaving size and an 8-fold increase in the transport rate.[110] This is due to the synergistic combination of the surface properties of SLIPS and mechanical actuation. In 2021, they have explored the life span of SLIPS during condensation.[111] Studies have shown that surfaces impregnated with higher viscosity oils (5216 mPa s) will increase the life of SLIPS and maintain good stability in steam at 200 °C. Vapor shear tests show that SLIPSs do not suffer oil depletion when exposed to 10 m s^{-1} gas flow, which is critical for the implementation of condensers where single-phase superheated steam impingement is prevalent. In 2022, Muhammad *et al.* explored the life span of the lubricant layer on SLIPS during steam condensation and found that by increasing the molecular weight of the lubricant, the life can be extended from 1 month to 8 months.[111] In 2022, Guo *et al.* developed a novel model of droplet condensation kinetics on hydrophilic SLIPS, which takes into account the droplet disappearance phenomenon caused by coarsening and provides a theoretical basis for designing condensing surfaces.[112]

3.6 Fog collection

The collection of fog in nature is valuable to relieve the global water shortage crisis. SLIPS performs excellently in fog collection due to the molecular smoothness of its surface. Back in 2013, Lalia *et al.* fabricated lubricant-impregnated electrospun

 This journal is © The Royal Society of Chemistry 2023

Published on 04 2023. Downloaded on 31.01.2026 01:32:34.

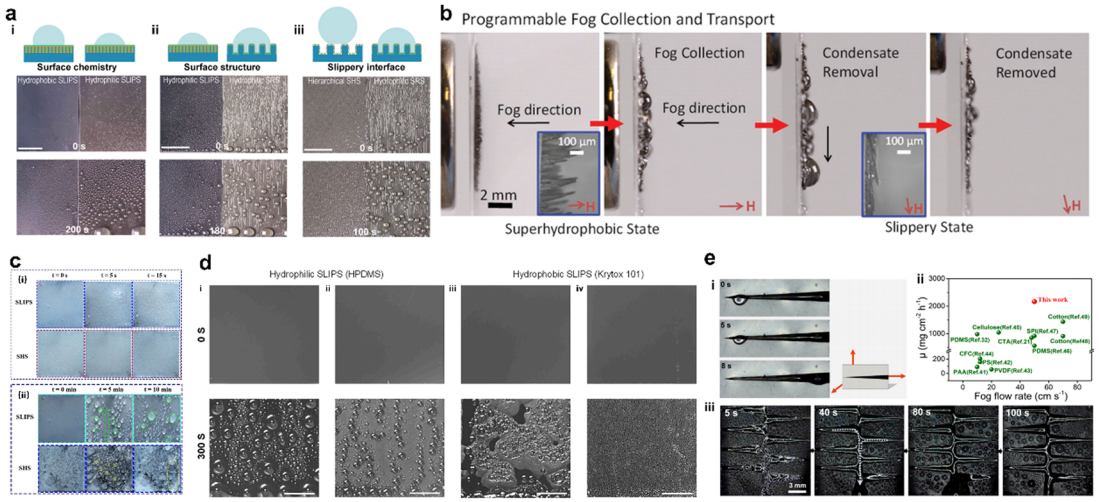

Fig. 12 Promoting fog collection with SLIPS. (a) Dropwise condensation on (i) hierarchical SHS, (ii) hydrophilic SLIPS, and (iii) hydrophilic directional SRS.[24] (b) Programmable fog collection and transport: the transformable surface was placed normal to the direction of the incoming fog. In the superhydrophobic state, the micropillars collect the fog from air utilizing their high surface area.[22] (c) (i) Images of the fog capture process of the SLIPS and SHS at 5 and 15 s. (ii) Images of the water harvesting process of the SLIPS and SHS at 5 and 10 min.[115] (d) (i and ii) Water harvesting performance on hydrophilic SLIPS (HPDMS) during the dew harvesting test on (i) 9.1 mm lubricant thickness and (ii) 3.0 mm lubricant thickness. The rapid formation of large-size droplets on the thicker lubricant results from the stronger coarsening effect. (iii and iv) Water harvesting performance on hydrophobic SLIPS (Krytox 101) during the dew harvesting test on (iii) 9.1 mm lubricant thickness and (iv) 3.0 mm lubricant thickness. No large droplet was formed due to the weak coarsening effect.[114] (e) Needle-like superhydrophilic SLIPSs that can significantly improve the collection efficiency of fog.[118]

nanomaterials that exhibited higher water collection rates than unimpregnated lubricant samples.[113] In 2017, Huang *et al.* prepared a surface consisting of SLIPS and a superhydrophobic surface for mist collection that could be magnetically converted between the two states.[22] When the surface is superhydrophobic, it facilitates the accumulation and condensation of mist, and when it is in a slippery state, it facilitates the removal of liquid droplets. In 2018, Dai *et al.* introduced oriented microgrooves into SLIPS and presented a hydrophilic directional slippery rough surface.[24] Due to its large surface area, hydrophilic slippery interface, and directional fluid driving properties, it performed excellently in fog collection. The authors later further investigated the mechanism of hydrophilic slippery surfaces in the process of fog collection.[114] They found meniscus-mediated spontaneous droplet climbing and rapid droplet merging on hydrophilic slippery surfaces and characterized this as a coarsening effect. In 2021, Guo *et al.* then prepared a WO_3-based SLIPS by spraying method and photocatalytic reaction method (Fig. 12c).[115] This SLIPS showed excellent performance in mist capture, water droplet condensation and water droplet removal. In 2021, Cheng *et al.* constructed a smooth "anti-fog brush" with an aluminum oxide microneedle structure surface. As a droplet passes through the sample in an arc pattern, it will completely contact the surface, with only a few droplets escaping from the surface. As adjacent droplets agglomerate, the droplets slide along both sides of the pattern, and then the contact surface decreases from tip to base so that droplets can be transported quickly.[116] In 2022, Li *et al.* proposed a PDMS electric brush to treat SLIPS surfaces that could achieve a water droplet limit removal that was an order of magnitude smaller than that in air.[117] Yu-Zhong Wang and co-workers designed a spontaneous fog collection system based on SLIPS with superhydrophilic surfaces and fully optimized the four collection steps in terms of improved fog capture, promotion of microdroplet orientation aggregation, accelerated water transport, and reduction of water collection barriers. The water collection efficiency is high up to 2166 ± 71 mg cm^{-2} h^{-1}, which is 139% higher compared to a uniform SLIPS (Fig. 12e).[118]

3.7 Anti-icing

In some scenarios, water icing can endanger the normal life of human beings, such as the icing on roads, the icing on power lines, the icing on power transmission towers and icing on planes. The SLIPS exhibits excellent icephobicity due to its unique surface properties. In 2012, Kim *et al.* demonstrated for the first time the potential of SLIPSs for anti-icing applications.[48] The authors explored the formation of frost and ice on SLIPS prepared on aluminum surfaces and found that ice on their surfaces would easily fall off due to their extremely low contact angle hysteresis. According to the report of Lv *et al.* in 2014, the homogeneity of the SLIPS surface with few nucleation sites due to molecular smoothness can effectively inhibit the formation of ice on its surface.[119] Zhu *et al.* investigated the effect of the thickness of the silicone oil layer on the surface of PDMS on the anti-icing performance.[120] The thickness of the silicone oil layer was found to be proportional to the anti-icing capability, which was related to better coverage of its surface silicone oil as the amount of silicone oil increased. Rykaczewski *et al.* made a detailed observation of the process of ice frost formation on the SLIPS surface with the aid of cryogenic scanning electron microscopy.[31] The finding that the lubricant layer on the surface of micron-sized rough

Published on 04 2023. Downloaded on 31.01.2026 01:32:34.

substrates is replaced by ice indicates that the anti-icing effect of SLIPS on micron-sized rough substrates is not very satisfactory. Later, Subramanyam *et al.* reported that the adhesion strength of ice on SLIPS surfaces depends on the texture of the substrate and is inversely proportional to the texture density, indicating the critical role of substrates with nanoscale roughness in SLIPS anti-icing applications.[121] In 2014, Dou *et al.* demonstrated for the first time that ice formed on the surface of the anti-icing SLIPS could be blown away by the action of wind in a wind tunnel with controlled temperature and wind speed, and in addition, low ice viscosity can be maintained even when the temperature is lowered to −53 °C.[122] In 2015, Urata *et al.* reported a self-lubricating organogel with almost no ice adhesion on PDMS-based SLIPS surfaces (*ca.* 0.4 kPa), which is much less than the ice-resistant SLIPSs reported so far (*ca.* 15 kPa).[123] In 2016, Tuteja *et al.* systematically explored the two main factors, crosslink density, and interfacial slip, that can be used to systematically tailor ice adhesion to various elastomer surfaces and found that interfacial slip has the greatest effect on the ice adhesion strength of low crosslink density elastomers.[21] Utilizing this understanding, the authors fabricated a range of different, mechanically durable, and long-lasting ice-phobic surfaces from a wide range of material systems. This will promote the application of anti-icing SLIPSs in a wide range of industrial sectors, disciplines, and engineering fields (Fig. 13).

3.8 Anti-biofouling

Biological contamination is a difficult challenge in some medical appliances, ship hulls, and other marine infrastructures.[124] And, SLIPSs are expected to exhibit repellency to living cells, bacteria, and microorganisms due to their liquid repellency, liquid-like properties, molecularly smooth surfaces, and self-healing properties. In 2012, Aizenberg *et al.* demonstrated for the first time that the adhesion of Pseudomonas aeruginosa, Staphylococcus aureus, and *Escherichia coli* biofilms to the SLIPS was greatly reduced compared to that of Teflon or PEGlyated surfaces.[125] In 2014, Yao *et al.* prepared a series of fluorogel-swollen SLIPSs and explored the adhesion of BSA proteins and cells on their surfaces.[54] The SLIPS showed significant rejection of various biological fluids and maintained biocompatibility, indicating their potential application *in vivo*. Leslie *et al.* showed the potential of SLIPSs for medical device applications based on the biofouling resistance exhibited by SLIPSs.[14] They prepared a SLIPS coating on a medical-grade tube and catheter that prevents fibrin adhesion (Fig. 14a), reduces platelet adhesion and activation (Fig. 14e), inhibits biofilm formation (Fig. 14f), and remains stable under *in vitro* blood flow. They assembled catheters and conduits into arteriovenous shunts and implanted them in pigs, and worked for at least 8 hours without observing coagulation. This seminal work has provided additional possibilities for the development of medical devices that are anticoagulant as well as resistant to biological contamination. Tesler's bacterial culture experiments showed good resistance of SLIPSs to marine algal, blood, *Escherichia coli*, and *P. aeruginosa*.[49] Then, Yong demonstrated that the SLIPS has a good resistance to C6 glioma cells (Fig. 14d).[52] In 2017, Sunny *et al.* explored the activity of cells on the SLIPS.[126] The cells extend and contract filamentous

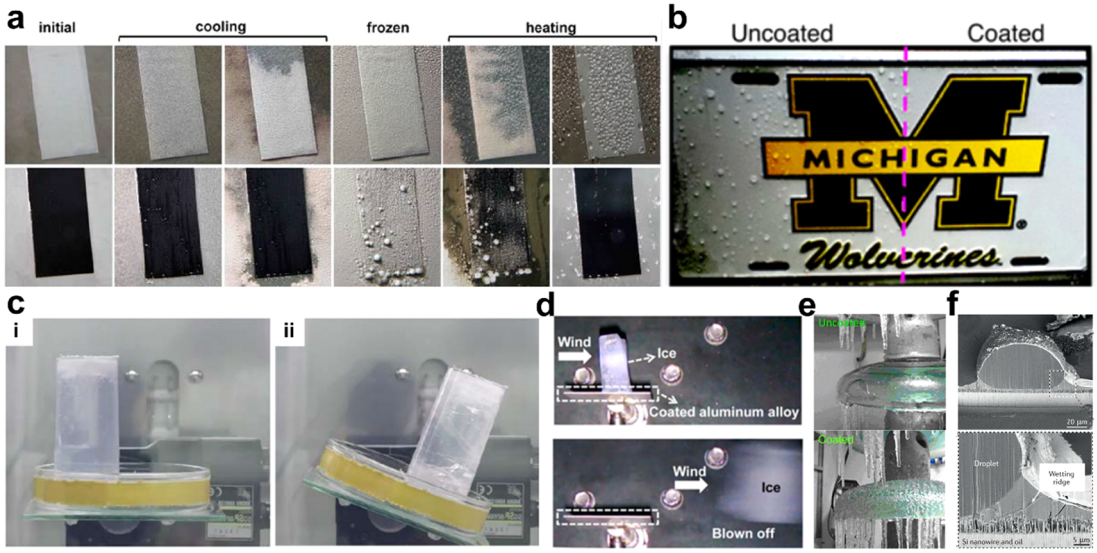

Fig. 13 Anti-icing with SLIPS. (a) The comparison of anti-icing performance between the original aluminum and the aluminum with a slippery coating. The records clearly showed that the slippery coating not only prevents the ice nucleation on the surface but also promotes the removal of melty ice.[48] (b) Half-coated license plate during outdoor winter 2013 testing, with ice only accreted on the uncoated side.[21] (c) Anti-icing properties of organogels prepared on Petri dishes (AR20 and TSF437 were mixed as organic phases).[123] (d) Effectiveness of the anti-icing coating with an aqueous lubricating layer was tested in the wind tunnel. The ice on the anti-icing could be blown off with a strong breeze. Arrows denote the direction of the wind.[122] (e) Ice formed on PDMS coated and uncoated surfaces of an insulator under a condensing weather condition at −5 °C and saturated humidity.[120] (f) The cryogenic scanning electron microscope images revealed that the infused liquid may cloak the droplet during the icing formation, indicating a possible reason for the anti-icing property.[31]

 This journal is © The Royal Society of Chemistry 2023

Published on 04 2023. Downloaded on 31.01.2026 01:32:34.

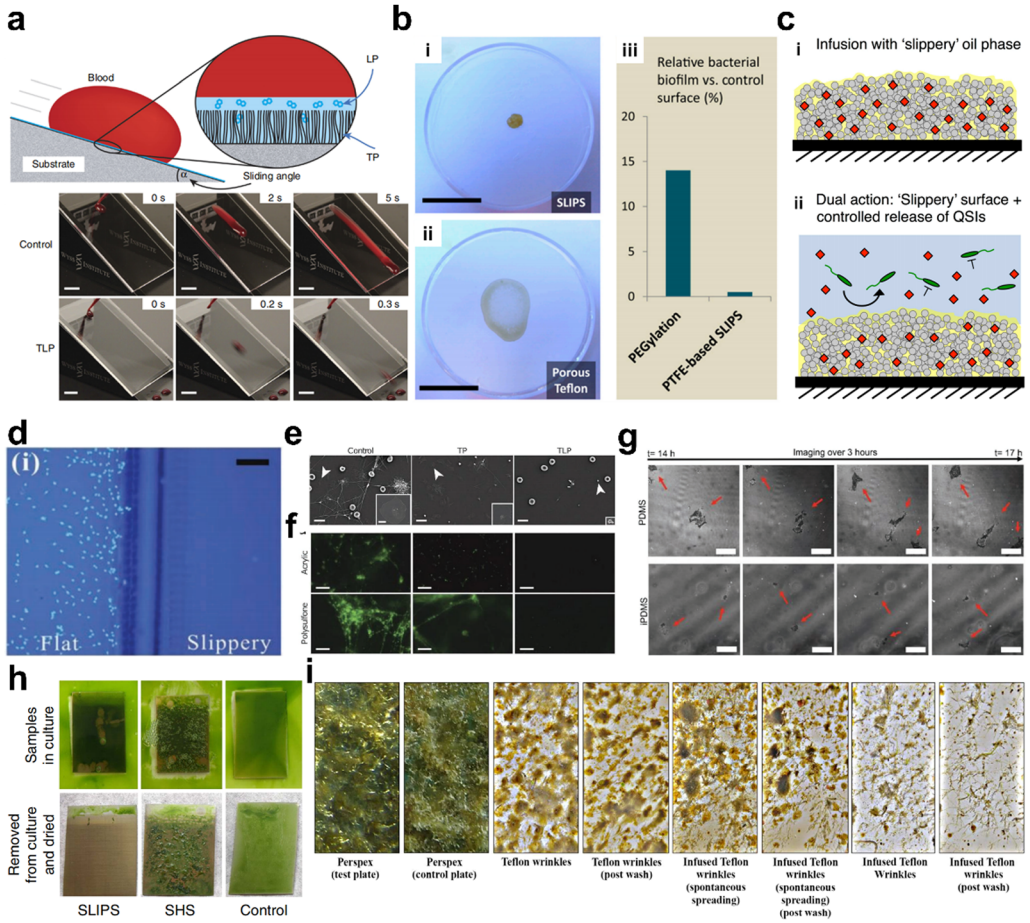

Fig. 14 Anti-biological contamination with SLIPS. (a) The slippery surface can effectively shield against the whole blood, indicating its promising application *in vivo*.[14] (b) Bacteria bio-film did not spread on the slippery surface, but can easily contaminate the porous Teflon substrate.[125] (c) Schematic illustration showing the quorum sensing inhibitor (QSI)-loaded liquid-infused surfaces. (d) Comparison of C6 glioma cell behavior at the boundaries between flat area and laser-induced roughened, fluoroalkylsilane-modified slippery surface. Scale bar 100 μm.[52] (e) SEM images of acrylic surfaces after 30 min incubation shows reduced platelet adhesion on a liquid-infused surface (TLP) compared to control and hydrophobic (TP) surfaces. Scale bars, 10 μm.[14] (f) Fluorescent micrographs of acrylic (upper panels) or polysulfone (lower panels) pieces (11 × 8 mm) after 90 min incubation with fresh human blood containing heparin (0.25 U ml^{-1}) and fluorescent fibrinogen (150 μg ml^{-1}) showing polymerized fibrin networks on the control (left), decreased network formation on TP (middle) and punctate staining with minimal network formation on TLP (right). Scale bars, 50 μm.[14] (g) Neonatal dermal fibroblasts imaged 14 h after seeding. The cells on PDMS were attaching and spreading, whereas the cells on infused PDMS (iPDMS) continued to probe the surface and secrete tethers but did not attach. All scale bars are 50 μm. Red arrows indicate the cells that are traversing and exploring the surface.[126] (h) The samples just before (top panels) and after (bottom panels) being removed from the culture and dried: TO-SLIPS, TO-SHS and untreated stainless-steel control.[49] (i) Optical images of fouled surfaces, after seven weeks of testing in the ocean, and after being washed.[129]

pseudopods as they probe and move across the liquid surface, and the range of filamentous pseudopods on the PDMS surface (100 μm) is much larger than that on the SLIPS surface (20 μm), indicating that cell motility on SLIPS is restricted (Fig. 14g). In 2018, Sun *et al.* proposed a method to prepare SLIPS on metal surfaces that can significantly improve the corrosion resistance of metal surfaces and have a droplet roll angle of less than 5°.[127] In 2020, Chen *et al.* first introduced a unique grafting fluid lubrication strategy by covalently grafting highly flexible polydimethylsiloxane (PDMS) brushes onto membranes, which can reduce contaminant adhesion and provide significant improvements in permeation flux and the superior antifouling ability for highly viscous organic liquids (*i.e.*, crude oil).[128] Ware *et al.* conducted a systematic exploration of the minimum lubricant use for SLIPS for anti-bacterial contamination, and at this lubricant use, the amount of lubricant lost was also minimal.[129] This offers good prospects for achieving a sustainable and benign surface resistant to contamination.

3.9 Liquid-based gating mechanism

Using a liquid as a structural material that responds to an applied force is not possible at the macroscopic level because liquids are too fluid and the forces between molecules are not as strong as those of solid materials. In contrast, at the microscopic scale, liquids can be stable if they are confined to a finite space by capillary forces. SLIPSs, which consist of porous membranes and lubricants, are able to achieve this effect. In 2015, Hou *et al.* proposed a liquid-based gating mechanism.[18] It uses a capillary-stabilized liquid as a

Published on 04 2023. Downloaded on 31.01.2026 01:32:34.

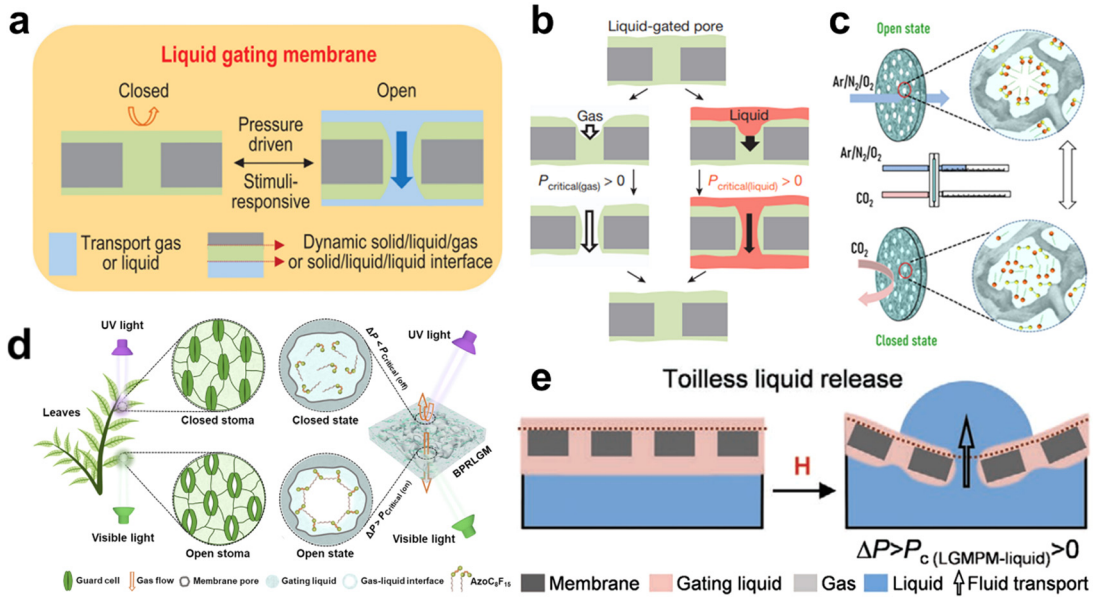

Fig. 15 Liquid-based gating mechanism. (a) The liquid gating membrane can use a capillary-stabilized functional gating liquid to form reversible gates inside the porous membranes.[26] (b) Hypothesis for gating a pore by liquid reconfiguration.[18] (c) Illustration of the switchable mechanism of the CO_2-CRSV.[28] (d) The bioinspired photo-responsive gating membrane of BPRLGM.[130] (e) Schematics of liquid gating magnetoelastic porous membrane and self-driven liquid release.[27]

reversible, reconfigurable gating mechanism that enables different response profiles for various liquids and gases by reasonably adjusting the gating threshold-the pressure required to open the pore-over a wide range, even allowing the liquid to flow through the pore while preventing the gas from escaping. This is of great interest for the development of systems capable of controlling complex and selective multiphase transport. In 2022, Lei *et al.* proposed an adaptive CO_2 gas valve consisting of a chemically reactive liquid gate system.[28] The critical pressure across the membrane of the liquid gate varies with the presence of carbon dioxide due to the assembly of a super-amphiphilic compound of poly(propylene glycol) bis(2-aminopropyl ether) and oleic acid in the gate liquid that is specifically protonated by carbon dioxide. It was shown that the valve could be adaptively regulated for specific gases and different concentrations of carbon dioxide. This protonation-induced liquid gating mechanism opens a potential platform for applications such as carbon dioxide separators, detectors, and sensors. In 2022, inspired by the leaves of plants, Zhang *et al.* created a bioinspired photo-responsive liquid-gating membrane by dissolving azobenzene-based photosensitive molecules into a nylon porous substrate. This material can be reversibly switched between closed and open states under different photo stimuli.[130] Liu *et al.* introduced the magnetic response into the liquid-based gating mechanism and designed a new system based on a liquid-gated magnetoelastic porous membrane with reversible meniscus-shaped deformation.[27] The advantage of this magneto responsive self-driven system is that it provides a general and convenient method for achieving active regulation of gas–liquid release. In addition, the system can be used to fully turn gas delivery on and off, reducing the gating pressure threshold for liquid release under the same conditions (Fig. 15).

4 Summary and outlook

Inspired by the pitcher plant, SLIPS is a new liquid-repellent surface consisting of a liquid lubricant and a solid substrate. Its particular mechanism of using liquids to repel liquids allows it to exhibit a series of excellent properties such as durable liquid repulsion, extremely low contact angle hysteresis, pressure resistance, and self-healing properties. SLIPSs with different unique properties can be easily prepared on a variety of material surfaces under the conditions of the preparation principles, which has facilitated the application of SLIPSs in various research and industrial fields. In recent years, SLIPS has shown great potential for applications in droplet manipulation, bubble manipulation, condensation, fog collection, anti-icing, anti-biological contamination, self-healing, liquid gates, *etc.*

As a stable hydrophobic and aerophilic surface, the manipulation of droplet and bubble behavior is achieved by combining it with patterns with different wettability and asymmetric structures using asymmetric Laplacian pressure. The dynamic manipulation of droplet motion behavior can also be achieved by introducing responsiveness into the lubricant or substrate. However, more ways to manipulate water droplets and bubbles remain to be developed, like combining more complex surface structures and response effects with SLIPS to achieve more complex applications, such as microfluidics, gas absorption, and multiphase reactions.

 This journal is © The Royal Society of Chemistry 2023

Published on 04 2023. Downloaded on 31.01.2026 01:32:34.

In addition, the SLIPS, as a surface capable of generating electricity by water droplets, shows a good prospect for sustainable energy production. The higher heat transfer efficiency of the SLIPS due to its dropwise condensation mode, combined with the extremely low contact angle hysteresis, makes the SLIPS a potential substrate that can be used for condensation and fog collection. It is foreseen that by optimizing the various components of SLIPSs – substrate material, substrate shape, lubricant selection, lubricant dosage, *etc.* are possible to achieve higher condensation and fog collection efficiency. Many reports have highlighted the excellent performance of SLIPSs in biological contamination prevention, as well as its application in the direction of medical devices. If the problem of lubricants being hazardous to the human body can be solved, the applicability of the SLIPS in the human body will be greatly increased, such as the realization of artificial joints, drug delivery, and tissue integration. Based on the SLIPS, Hou Xu *et al.* ingeniously designed a liquid-based gating mechanism. The lubricant is fixed in the pore by using capillary force to become a gate capable of phase separation as well as selective gas passage. This liquid-based gating mechanism is very novel and highly plastic, and the introduction of more responsiveness allows for more complex functions, such as the introduction of protein or ion responsiveness for cell membrane-like selective permeability, *etc.* Furthermore, similar to SLIPSs, solid-state super-lubricated surfaces with silanes bonded to the solid surface also have a range of SLIPS benefits and gain in stability.[131–133]

SLIPS has made a series of progress in both academic research and commercial products. However, to be honest, there are still some problems that restrict the wide application of SLIPSs. First of all, many (not all) reported SLIPSs are complicated in the preparation process, and it is necessary to prepare the porous substrate, modify the substrate, and then inject a lubricant. This makes the preparation cost of SLIPSs expensive and difficult to be produced on a large scale. Therefore, it is an urgent problem to develop a simpler and cheaper preparation process for SLIPSs in the process of industrialization.

Although the lubricant layer in the SLIPS is much more stable than the gas film on the superhydrophobic surface, the loss of lubricant is indeed an important problem that limits the application of SLIPSs, which should be emphasized. (1) Firstly, in long-term work, the lubricating layer may be exhausted due to the cloaking layer or the wetting ridge and other reasons, resulting in the loss of ''sliding'' characteristics of the SLIPS. In order to solve the problem of lubricant loss, researchers have made various explorations. In 2021, Kim *et al.* explored the loss of lubricant in the SLIPS porous substrate under the impact of continuous water flow.[134] The loss rate of lubricant will increase at first and then decrease until the lubricant is completely lost. Through this experiment, they found that the spherical cavity has better performance in retaining the lubricant because this shape can reduce the shear stress caused by water flow. In 2018, Pham *et al.* found that droplet cloaking takes time, so enlarging the droplet volume and reducing the droplet contact time is also an effective way to reduce the loss of the lubricant.[135] In addition, the loss of the lubricant can be correspondingly reduced by increasing the interaction between the lubricant and the porous substrate, such as selecting perfluoropolyether as a lubricant which is compatible with the hydrophobic porous substrate[136] or grafting the lubricant onto the solid substrate.[50] (2) Secondly, evaporation of lubricants really exists, for example, the boiling point of polydimethylsiloxane is about 200 °C, the boiling point of amino silicone oil is only 150 °C, *etc.*, which limits the use of SLIPSs in a high-temperature environment. For solving the problem of lubricant loss due to evaporation, lubricants with higher molecular weight and higher communication degrees or ionic liquids can be selected to reduce the volatility of lubricants. For example, 1-ethyl-3-methylimidazolium bis(trifluoromethylsulfonyl)imide can be heated at 250 °C for 12 hours without volatilization.[65] In 2022, Wang *et al.* reported a nanoscale ionic liquid with better thermal stability compared to perfluoropolyether, able to tolerate high temperatures approaching 300 °C.[137] (3) SLIPS also has a problem that the use of lubricants may pollute the environment. For example, some lubricants used in SLIPSs are fluorinated liquids, which might be hardly degraded and harmful to the organism, so it is necessary to find more eco-friendly and biocompatible substitutes to replace them.

Nature is always a school for human beings. The pitcher plant-inspired slippery surface has emerged with excellent properties such as liquid repellence, pressure tolerance, and self-replenishment. The movable lubricant layer endows the surface with flexible functions, and meanwhile diversifies the design approaches of such surface. Taking the advantage of the unique interface of a slippery surface, fluid can be easily and efficiently manipulated in accordance with the surface decoration. We envision that this review article can provide an overview of the fluid controlling process on multifunctional slippery surfaces, and also enlighten the optimization of the current systems relating to fluid/surface multiphase interaction.

Conflicts of interest

The authors declared no conflict of interest.

Acknowledgements

This work was supported by the National Natural Science Foundation of China (22075202, 21805204), the Haihe Laboratory of Sustainable Chemical Transformations, and the Young Elite Scientists Sponsorship Program by Tianjin (TJSQNTJ-2018-17).

References

1 H. F. Bohn and W. Federle, *Proc. Natl. Acad. Sci. U. S. A.*, 2004, **101**, 14138–14143.
2 A. Marmur, *Langmuir*, 2004, **20**, 3517–3519.

Published on 04 2023. Downloaded on 31.01.2026 01:32:34.

3 L. Zhai, F. C. Cebeci, R. E. Cohen and M. F. Rubner, *Nano Lett.*, 2004, **4**, 1349–1353.
4 X. Gao and L. Jiang, *Nature*, 2004, **432**, 36.
5 X.-Q. Feng, X. Gao, Z. Wu, L. Jiang and Q.-S. Zheng, *Langmuir*, 2007, **23**, 4892–4896.
6 L. Feng, Y. Zhang, J. Xi, Y. Zhu, N. Wang, F. Xia and L. Jiang, *Langmuir*, 2008, **24**, 4114–4119.
7 B. Bhushan and E. K. Her, *Langmuir*, 2010, **26**, 8207–8217.
8 G. D. Bixler and B. Bhushan, *Nanoscale*, 2013, **5**, 7685–7710.
9 U. Bauer and W. Federle, *Plant Signaling Behav.*, 2009, **4**, 1019–1023.
10 H. Chen, P. Zhang, L. Zhang, H. Liu, Y. Jiang, D. Zhang, Z. Han and L. Jiang, *Nature*, 2016, **532**, 85–89.
11 T. S. Wong, S. H. Kang, S. K. Y. Tang, E. J. Smythe, B. D. Hatton, A. Grinthal and J. Aizenberg, *Nature*, 2011, **477**, 443–447.
12 H. L. Liu, P. C. Zhang, M. J. Liu, S. T. Wang and L. Jiang, *Adv. Mater.*, 2013, **25**, 4477–4481.
13 X. Yao, Y. H. Hu, A. Grinthal, T. S. Wong, L. Mahadevan and J. Aizenberg, *Nat. Mater.*, 2013, **12**, 529–534.
14 D. C. Leslie, A. Waterhouse, J. B. Berthet, T. M. Valentin, A. L. Watters, A. Jain, P. Kim, B. D. Hatton, A. Nedder and K. Donovan, *Nat. Biotechnol.*, 2014, **32**, 1134–1140.
15 P. C. Zhang, H. L. Liu, J. X. Meng, G. Yang, X. L. Liu, S. T. Wang and L. Jiang, *Adv. Mater.*, 2014, **26**, 3131–3135.
16 X. Yao, J. Ju, S. Yang, J. Wang and L. Jiang, *Adv. Mater.*, 2014, **26**, 1895–1900.
17 U. Manna and D. M. Lynn, *Adv. Mater.*, 2015, **27**, 3007–3012.
18 X. Hou, Y. Hu, A. Grinthal, M. Khan and J. Aizenberg, *Nature*, 2015, **519**, 70–73.
19 C. Hao, J. Li, Y. Liu, X. Zhou, Y. Liu, R. Liu, L. Che, W. Zhou, D. Sun, L. Li, L. Xu and Z. Wang, *Nat. Commun.*, 2015, **6**, 7986.
20 K. C. Park, P. Kim, A. Grinthal, N. He, D. Fox, J. C. Weaver and J. Aizenberg, *Nature*, 2016, **531**, 78–82.
21 K. Golovin, S. P. Kobaku, D. H. Lee, E. T. DiLoreto, J. M. Mabry and A. Tuteja, *Sci. Adv.*, 2016, **2**, e1501496.
22 Y. Huang, B. B. Stogin, N. Sun, J. Wang, S. Yang and T. S. Wong, *Adv. Mater.*, 2017, **29**, 1604641.
23 M. Cao, X. Jin, Y. Peng, C. Yu, K. Li, K. Liu and L. Jiang, *Adv. Mater.*, 2017, **29**, 1606869.
24 X. Dai, N. Sun, S. O. Nielsen, B. B. Stogin, J. Wang, S. Yang and T.-S. Wong, *Sci. Adv.*, 2018, **4**, eaaq0919.
25 X. Liu, H. Gu, M. Wang, X. Du, B. Gao, A. Elbaz, L. Sun, J. Liao, P. Xiao and Z. Gu, *Adv. Mater.*, 2018, **30**, 1800103.
26 X. Hou, *Natl. Sci. Rev.*, 2020, **7**, 9–11.
27 J. Liu, X. Xu, Y. Lei, M. Zhang, Z. Sheng, H. Wang, M. Cao, J. Zhang and X. Hou, *Adv. Mater.*, 2022, **34**, 2107327.
28 J. Lei, Y. Hou, H. Wang, Y. Fan, Y. Zhang, B. Chen, S. Yu and X. Hou, *Angew. Chem., Int. Ed.*, 2022, **61**, e202201109.
29 L. Xiao, J. Li, S. Mieszkin, A. Di Fino, A. S. Clare, M. E. Callow, J. A. Callow, M. Grunze, A. Rosenhahn and P. A. Levkin, *ACS Appl. Mater. Interfaces*, 2013, **5**, 10074–10080.
30 N. Vogel, R. A. Belisle, B. Hatton, T.-S. Wong and J. J. N. C. Aizenberg, *Nat. Commun.*, 2013, **4**, 1–10.
31 K. Rykaczewski, S. Anand, S. B. Subramanyam and K. K. Varanasi, *Langmuir*, 2013, **29**, 5230–5238.
32 J. Zhang, A. Wang and S. Seeger, *Adv. Funct. Mater.*, 2014, **24**, 1074–1080.
33 J. Li, E. Ueda, D. Paulssen and P. A. Levkin, *Adv. Funct. Mater.*, 2019, **29**, 1802317.
34 S. Peppou-Chapman, J. K. Hong, A. Waterhouse and C. Neto, *Chem. Soc. Rev.*, 2020, **49**, 3688–3715.
35 W. He, P. Liu, J. Zhang and X. Yao, *Chem. – Eur. J.*, 2018, **24**, 14864–14877.
36 R. Deng, T. Shen, H. Chen, J. Lu, H.-C. Yang and W. Li, *J. Mater. Chem. A*, 2020, **8**, 7536–7547.
37 C. Howell, A. Grinthal, S. Sunny, M. Aizenberg and J. Aizenberg, *Adv. Mater.*, 2018, **30**, 1802724.
38 M. Cao, D. Guo, C. Yu, K. Li, M. Liu and L. Jiang, *ACS Appl. Mater. Interfaces*, 2016, **8**, 3615–3623.
39 D. J. Preston, Y. Song, Z. Lu, D. S. Antao and E. N. J. A. A. M. Wang and interfaces, *ACS Appl. Mater. Interfaces*, 2017, **9**, 42383–42392.
40 D. Daniel, J. V. Timonen, R. Li, S. J. Velling and J. Aizenberg, *Nat. Phys.*, 2017, **13**, 1020–1025.
41 B. Li and K. Li, *Appl. Surf. Sci.*, 2022, 153782.
42 X. Chen, G. Wen and Z. Guo, *Mater. Horiz.*, 2020, **7**, 1697–1726.
43 X. Wang, J. Huang and Z. Guo, *Adv. Colloid Interface Sci.*, 2022, 102602.
44 H. Bazyar, O. A. Moultos and R. G. Lammertink, *J. Chem. Phys.*, 2022, **157**, 144704.
45 C. Zhang, B. Zhang, H. Ma, Z. Li, X. Xiao, Y. Zhang, X. Cui, C. Yu, M. Cao and L. Jiang, *ACS Nano*, 2018, **12**, 2048–2055.
46 U. Manna and D. M. Lynn, *Adv. Mater.*, 2015, **27**, 3007–3012.
47 K. Zhuang, X. Yang, W. Huang, Q. Dai and X. Wang, *ACS Appl. Mater. Interfaces*, 2021, **13**, 61780–61788.
48 P. Kim, T. S. Wong, J. Alvarenga, M. J. Kreder, W. E. Adorno-Martinez and J. Aizenberg, *ACS Nano*, 2012, **6**, 6569–6577.
49 A. B. Tesler, P. Kim, S. Kolle, C. Howell, O. Ahanotu and J. Aizenberg, *Nat. Commun.*, 2015, **6**, 1–10.
50 R. Xiao, N. Miljkovic, R. Enright and E. N. Wang, *Sci. Rep.*, 2013, **3**, 1988.
51 J. Yong, F. Chen, Q. Yang, Y. Fang, J. Huo, J. Zhang and X. Hou, *Adv. Mater. Interfaces*, 2017, **4**, 1700552.
52 J. Yong, J. Huo, Q. Yang, F. Chen, Y. Fang, X. Wu, L. Liu, X. Lu, J. Zhang and X. Hou, *Adv. Mater. Interfaces*, 2018, **5**, 1701479.
53 A. C. Glavan, R. V. Martinez, A. B. Subramaniam, H. J. Yoon, R. M. Nunes, H. Lange, M. M. Thuo and G. M. Whitesides, *Adv. Funct. Mater.*, 2014, **24**, 60–70.
54 X. Yao, S. S. Dunn, P. Kim, M. Duffy, J. Alvarenga and J. Aizenberg, *Angew. Chem., Int. Ed.*, 2014, **53**, 4418–4422.
55 I. Okada and S. J. A. A. M. Shiratori and interfaces, *ACS Appl. Mater. Interfaces*, 2014, **6**, 1502–1508.
56 A. Eifert, D. Paulssen, S. N. Varanakkottu, T. Baier and S. Hardt, *Adv. Mater. Interfaces*, 2014, **1**, 1300138.
57 J. Guo, W. Fang, A. Welle, W. Feng, I. Filpponen, O. J. Rojas and P. A. Levkin, *ACS Appl. Mater. Interfaces*, 2016, **8**, 34115–34122.

 This journal is © The Royal Society of Chemistry 2023

Published on 04 2023. Downloaded on 31.01.2026 01:32:34.

58 Z. Dong, M. F. Schumann, M. J. Hokkanen, B. Chang, A. Welle, Q. Zhou, R. H. Ras, Z. Xu, M. Wegener and P. A. Levkin, *Adv. Mater.*, 2018, **30**, 1803890.
59 Q. Wei, C. Schlaich, S. Prévost, A. Schulz, C. Böttcher, M. Gradzielski, Z. Qi, R. Haag and C. A. Schalley, *Adv. Mater.*, 2014, **26**, 7358–7364.
60 C. Howell, T. L. Vu, J. J. Lin, S. Kolle, N. Juthani, E. Watson, J. C. Weaver, J. Alvarenga and J. Aizenberg, *ACS Appl. Mater. Interfaces*, 2014, **6**, 13299–13307.
61 J. Cui, D. Daniel, A. Grinthal, K. Lin and J. Aizenberg, *Nat. Mater.*, 2015, **14**, 790–795.
62 H. Zhao, Q. Sun, X. Deng and J. Cui, *Adv. Mater.*, 2018, **30**, 1802141.
63 M. Tenjimbayashi, S. Nishioka, Y. Kobayashi, K. Kawase, J. Li, J. Abe and S. Shiratori, *Langmuir*, 2018, **34**, 1386–1393.
64 L. Sun, Y. Wang, X. Zhang, F. Bian, L. Shang, Y. Zhao and W. Sun, *Chem. Eng. J.*, 2021, **426**, 131641.
65 D. F. Miranda, C. Urata, B. Masheder, G. J. Dunderdale, M. Yagihashi and A. Hozumi, *APL Mater.*, 2014, **2**, 056108.
66 X. Meng, Z. Wang, L. Wang, L. Heng and L. Jiang, *J. Mater. Chem. A*, 2018, **6**, 16355–16360.
67 Y. Li, J. John, K. W. Kolewe, J. D. Schiffman and K. R. Carter, *ACS Appl. Mater. Interfaces*, 2015, **7**, 23439–23444.
68 G. H. Zhu, S.-H. Cho, H. Zhang, M. Zhao and N. S. Zacharia, *Langmuir*, 2018, **34**, 4722–4731.
69 H. Guo, P. Fuchs, K. Casdorff, B. Michen, M. Chanana, H. Hagendorfer, Y. E. Romanyuk and I. Burgert, *Adv. Mater. Interfaces*, 2017, **4**, 1600289.
70 C. Gao, L. Wang, Y. Lin, J. Li, Y. Liu, X. Li, S. Feng and Y. Zheng, *Adv. Funct. Mater.*, 2018, **28**, 1803072.
71 M. Tenjimbayashi, R. Togasawa, K. Manabe, T. Matsubayashi, T. Moriya, M. Komine and S. Shiratori, *Adv. Funct. Mater.*, 2016, **26**, 6693–6702.
72 H. Hu, G. Liu and J. Wang, *J. Mater. Chem. A*, 2019, **7**, 1519–1528.
73 T. Ni, J. Lin, L. Kong and S. Zhao, *Chin. Chem. Lett.*, 2021, **32**, 3298–3306.
74 J. Xu, S. Xiu, Z. Lian, H. Yu and J. Cao, *Droplet*, 2022, **1**, 11–37.
75 X. Leng, L. Sun, Y. Long and Y. Lu, *Droplet*, 2022, **1**, 139–169.
76 D. Paulssen, W. Feng, I. Pini and P. A. Levkin, *Adv. Mater. Interfaces*, 2018, **5**, 1800852.
77 P. Li, M. Cao, H. Bai, T. Zhao, Y. Ning, X. Wang, K. Liu and L. Jiang, *Adv. Funct. Mater.*, 2019, **29**, 1904446.
78 C. Hao, Y. Liu, X. Chen, Y. He, Q. Li, K. Li and Z. Wang, *Sci. Rep.*, 2014, **4**, 1–7.
79 Z. Cai, F. Chen, Y. Tian, D. Zhang, Z. Lian and M. Cao, *Chem. Eng. J.*, 2022, **449**, 137831.
80 Y. Lei, R. Sun, X. Zhang, X. Feng and L. Jiang, *Adv. Mater.*, 2016, **28**, 1477–1481.
81 Y. Wu, J. Feng, H. Gao, X. Feng and L. Jiang, *Adv. Mater.*, 2019, **31**, 1800718.
82 X. Zhang, C. Liu, L. Zhang, L. Jia, M. Shi, L. Chen, Y. Di and Z. Gan, *Adv. Funct. Mater.*, 2021, **31**, 2010406.
83 Z. Long, Y. Zhao, C. Zhang, Y. Zhang, C. Yu, Y. Wu, J. Ma, M. Cao and L. Jiang, *Adv. Mater.*, 2020, **32**, 1908099.
84 Y. Jeung and K. Yong, *Chem. Eng. J.*, 2020, **381**, 122734.
85 F. Liu, L. Wang, Q. Sun, L. Zhu, X. Meng and F.-S. Xiao, *J. Am. Chem. Soc.*, 2012, **134**, 16948–16950.
86 Q. Hao, C. Liu, G. Jia, Y. Wang, H. Arandiyan, W. Wei and B.-J. Ni, *Mater. Horiz.*, 2020, **7**, 1014–1029.
87 R. Shi, J. Guo, X. Zhang, G. I. Waterhouse, Z. Han, Y. Zhao, L. Shang, C. Zhou, L. Jiang and T. Zhang, *Nat. Commun.*, 2020, **11**, 1–10.
88 X. Sheng, Z. Liu, R. Zeng, L. Chen, X. Feng and L. Jiang, *J. Am. Chem. Soc.*, 2017, **139**, 12402–12405.
89 Y. Li, L. He, X. Zhang, N. Zhang and D. Tian, *Adv. Mater.*, 2017, **29**, 1703802.
90 X. Li, J. Zhang, X. Wang, D. Lv, C. Cao, L. Ai and X. Yao, *Droplet*, 2022, **1**, 65–75.
91 X. Liang, V. Kumar, F. Ahmadi and Y. Zhu, *Droplet*, 2022, **1**, 80–91.
92 C. Yu, X. Zhu, K. Li, M. Cao and L. Jiang, *Adv. Funct. Mater.*, 2017, **27**, 1701605.
93 X. Tang, H. Xiong, T. Kong, Y. Tian, W.-D. Li and L. Wang, *ACS Appl. Mater. Interfaces*, 2018, **10**, 3029–3038.
94 G. Liu, C. Zhang, M. Liu, Z. Guo, X. Wang, C. Yu and M. Cao, *Trans. Tianjin Univ.*, 2020, **26**, 441–449.
95 A. M. Rather, Y. Xu, Y. Chang, R. L. Dupont, A. Borbora, U. I. Kara, J. C. Fang, R. Mamtani, M. Zhang and Y. J. A. M. Yao, *Adv. Mater.*, 2022, **34**, 2110085.
96 P. Guo, Z. Wang, L. Heng, Y. Zhang, X. Wang and L. Jiang, *Adv. Funct. Mater.*, 2019, **29**, 1808717.
97 C. Chen, H. Yao, Y. Jiao, C. Jia and S. Wu, *Langmuir*, 2022, **38**, 2174–2184.
98 X. Wang, H. Bai, J. Yang, Z. Li, Y. Wu, C. Yu, L. Jiang and M. Cao, *Small*, 2021, **17**, 2007803.
99 J. Zhang, P. Liu, B. Yi, Z. Wang, X. Huang, L. Jiang and X. Yao, *ACS Nano*, 2019, **13**, 10596–10602.
100 C. Zhang, X. Xiao, Y. Zhang, Z. Liu, X. Xiao, A. Nashalian, X. Wang, M. Cao, X. He and J. Chen, *ACS Nano*, 2022, **16**, 9348–9358.
101 N. Zhang, H. Zhang, W. Xu, H. Gu, S. Ye, H. Zheng, Y. Song, Z. Wang and X. Zhou, *Droplet*, 2022, **1**, 56–64.
102 Y. Song, W. Xu, Y. Liu, H. Zheng, M. Cui, Y. Zhou, B. Zhang, X. Yan, L. Wang, P. Li, X. Xu, Z. Yang and Z. Wang, *Innovation*, 2022, **3**, 100301.
103 F. Wang, M. Liu, C. Liu, Q. Zhao, T. Wang, Z. Wang and X. Du, *Sci. Adv.*, 2022, **8**, eabp9369.
104 W. Xu, X. Zhou, C. Hao, H. Zheng, Y. Liu, X. Yan, Z. Yang, M. Leung, X. C. Zeng, R. X. Xu and Z. Wang, *Natl. Sci. Rev.*, 2019, **6**, 540–550.
105 S. Anand, A. T. Paxson, R. Dhiman, J. D. Smith and K. K. Varanasi, *ACS Nano*, 2012, **6**, 10122–10129.
106 S. Anand, K. Rykaczewski, S. B. Subramanyam, D. Beysens and K. K. Varanasi, *Soft Matter*, 2015, **11**, 69–80.
107 K.-C. Park, P. Kim, A. Grinthal, N. He, D. Fox, J. C. Weaver and J. Aizenberg, *Nature*, 2016, **531**, 78–82.
108 S. Adera, J. Alvarenga, A. V. Shneidman, C. T. Zhang, A. Davitt and J. Aizenberg, *ACS Nano*, 2020, **14**, 8024–8035.
109 D. J. Preston, Z. Lu, Y. Song, Y. Zhao, K. L. Wilke, D. S. Antao, M. Louis and E. N. Wang, *Sci. Rep.*, 2018, **8**, 1–9.

Published on 04 2023. Downloaded on 31.01.2026 01:32:34.

110 I. Oh, H. Cha, J. Chen, S. Chavan, H. Kong, N. Miljkovic and Y. Hu, *ACS Nano*, 2020, **14**, 13367–13379.
111 M. J. Hoque, S. Sett, X. Yan, D. Liu, K. F. Rabbi, H. Qiu, M. Qureshi, G. Barac, L. Bolton and N. Miljkovic, *ACS Appl. Mater. Interfaces*, 2022, **14**, 4598–4611.
112 Z. Guo, D. Monga, L. Shan, D. Boylan and X. Dai, *Droplet*, 2022, **1**, 170–181.
113 B. S. Lalia, S. Anand, K. K. Varanasi and R. Hashaikeh, *Langmuir*, 2013, **29**, 13081–13088.
114 Z. Guo, L. Zhang, D. Monga, H. A. Stone and X. Dai, *Cell Rep. Phys. Sci.*, 2021, **2**, 100387.
115 H. Fan and Z. Guo, *J. Colloid Interface Sci.*, 2021, **591**, 418–428.
116 Y. Cheng, S. Zhang, S. Liu, J. Huang, Z. Zhang, X. Wang, Z. Yu, S. Li, Z. Chen and Y. Zhao, *J. Cleaner Prod.*, 2021, **315**, 127862.
117 S. Li, Y. Hou, M. Kappl, W. Steffen, J. Liu and H. J. Butt, *Adv. Mater.*, 2022, **34**, 2203242.
118 R. Feng, F. Song, C. Xu, X.-L. Wang and Y.-Z. Wang, *Chem. Eng. J.*, 2021, **422**, 130119.
119 J. Lv, Y. Song, L. Jiang and J. Wang, *ACS Nano*, 2014, **8**, 3152–3169.
120 L. Zhu, J. Xue, Y. Wang, Q. Chen, J. Ding and Q. Wang, *ACS Appl. Mater. Interfaces*, 2013, **5**, 4053–4062.
121 S. B. Subramanyam, K. Rykaczewski and K. K. Varanasi, *Langmuir*, 2013, **29**, 13414–13418.
122 R. M. Dou, J. Chen, Y. F. Zhang, X. P. Wang, D. P. Cui, Y. L. Song, L. Jiang and J. J. Wang, *ACS Appl. Mater. Interfaces*, 2014, **6**, 6998–7003.
123 C. Urata, G. J. Dunderdale, M. W. England and A. Hozumi, *J. Mater. Chem. A*, 2015, **3**, 12626–12630.
124 Z.-Z. Sheng, X. Liu, L.-L. Min, H.-L. Wang, W. Liu, M. Wang, L.-Z. Huang, F. Wu and X. Hou, *Chin. Chem. Lett.*, 2017, **28**, 1131–1134.
125 A. K. Epstein, T. S. Wong, R. A. Belisle, E. M. Boggs and J. Aizenberg, *Proc. Natl. Acad. Sci. U. S. A.*, 2012, **109**, 13182–13187.
126 S. Sunny, *Doctoral Dissertation*, Harvard University, 2017.
127 J. Sun, C. Wang, J. Song, L. Huang, Y. Sun, Z. Liu, C. Zhao and Y. Li, *J. Mater. Sci.*, 2018, **53**, 16099–16109.
128 L. Chen, Q. Feng, S. Huang, Z. Lin, J. Li and X. Tian, *J. Membr. Sci.*, 2020, **610**, 118240.
129 C. S. Ware, T. Smith-Palmer, S. Peppou-Chapman, L. R. Scarratt, E. M. Humphries, D. Balzer and C. Neto, *ACS Appl. Mater. Interfaces*, 2018, **10**, 4173–4182.
130 R. Zhang, J. Lei, J. Xu, H. Fu, Y. Jing, B. Chen and X. Hou, *Biomimetics*, 2022, **7**, 47.
131 X. Wang, Z. Wang, L. Heng and L. Jiang, *Adv. Funct. Mater.*, 2020, **30**, 1902686.
132 K. Han, Z. Wang, L. Heng and L. Jiang, *J. Mater. Chem. A*, 2021, **9**, 16974–16981.
133 S. Cheng, P. Guo, X. Wang, P. Che, X. Han, R. Jin, L. Heng and L. Jiang, *Chem. Eng. J.*, 2022, **431**, 133411.
134 H. N. Kim, S. J. Kim, W. Choi, H. J. Sung and S. J. Lee, *Phys. Fluids*, 2021, **33**, 022005.
135 Q. N. Pham, S. Zhang, K. Montazeri and Y. Won, *Langmuir*, 2018, **34**, 14439–14447.
136 P. Kim, M. J. Kreder, J. Alvarenga and J. Aizenberg, *Nano Lett.*, 2013, **13**, 1793–1799.
137 B. Wang, A. Tirado, F. Yang, C. Moran, M. Vander Woude, Y. Song, X. Wang, R. Qiao, S. Bai and Q. Guo, *Droplet*, 2022, **1**, 192–201.

 This journal is © The Royal Society of Chemistry 2023